Gene Identification for Ocular Congenital Cranial Motor Neuron Disorders Using Human Sequencing, Zebrafish Screening, and Protein Binding Microarrays

Julie A. Jurgens,[1–4] Paola M. Matos Ruiz,[2] Jessica King,[5] Emma E. Foster,[2] Lindsay Berube,[2] Wai-Man Chan,[1–4,6] Brenda J. Barry,[1,2,6] Raehoon Jeong,[5,7] Elisabeth Rothman,[5] Mary C. Whitman,[1,8,9] Sarah MacKinnon,[8,9] Cristina Rivera-Quiles,[2] Brandon M. Pratt,[2] Teresa Easterbrooks,[2] Fiona M. Mensching,[2] Silvio Alessandro Di Gioia,[1–4,10] Lynn Pais,[11,12] Eleina M. England,[11,12] Teresa de Berardinis,[13] Adriano Magli,[13] Feray Koc,[14] Kazuhide Asakawa,[15] Koichi Kawakami,[16] Anne O'Donnell-Luria,[11,12,17] David G. Hunter,[8,9] Caroline D. Robson,[18,19] Martha L. Bulyk,[4,5,7,20] and Elizabeth C. Engle[1–4,6,8,9]

[1]F.M. Kirby Neurobiology Center, Boston Children's Hospital, Boston, Massachusetts, United States
[2]Department of Neurology, Boston Children's Hospital, Boston, Massachusetts, United States
[3]Department of Neurology, Harvard Medical School, Boston, Massachusetts, United States
[4]Broad Institute of MIT and Harvard, Cambridge, Massachusetts, United States
[5]Division of Genetics, Department of Medicine, Brigham and Women's Hospital and Harvard Medical School, Boston, Massachusetts, United States
[6]Howard Hughes Medical Institute, Chevy Chase, Maryland, United States
[7]Bioinformatics and Integrative Genomics Graduate Program, Harvard University, Cambridge, Massachusetts, United States
[8]Department of Ophthalmology, Boston Children's Hospital, Boston, Massachusetts, United States
[9]Department of Ophthalmology, Harvard Medical School, Boston, Massachusetts, United States
[10]Regeneron Pharmaceuticals, Tarrytown, New York, United States
[11]Program in Medical and Population Genetics, Broad Institute of MIT and Harvard, Cambridge, Massachusetts, United States
[12]Division of Genetics and Genomics, Boston Children's Hospital, Harvard Medical School, Boston, Massachusetts, United States
[13]Department of Ophthalmologic Sciences, Faculty of Medicine and Surgery, University "Federico II", Naples, Italy
[14]Department of Ophthalmology, Faculty of Medicine, Izmir Katip Celebi University, Izmır, Turkey
[15]Neurobiology and Pathology Laboratory, National Institute of Genetics, Mishima, Shizuoka, Japan
[16]Laboratory of Molecular and Developmental Biology, National Institute of Genetics; Department of Genetics, Graduate University for Advanced Studies (SOKENDAI), Mishima, Shizuoka, Japan
[17]Center for Genomic Medicine, Massachusetts General Hospital, Boston, Massachusetts, United States
[18]Division of Neuroradiology, Department of Radiology, Boston Children's Hospital, Boston, Massachusetts, United States
[19]Department of Radiology, Harvard Medical School, Boston, Massachusetts, United States
[20]Department of Pathology, Brigham and Women's Hospital and Harvard Medical School, Boston, Massachusetts, United States

Correspondence: Elizabeth C. Engle, Boston Children's Hospital, Engle Lab-CLS14076 (BCH3149), 3 Blackfan St., Boston, MA 02115, USA; elizabeth.engle@childrens.harvard.edu.

Received: September 12, 2024
Accepted: February 24, 2025
Published: March 31, 2025

Citation: Jurgens JA, Matos Ruiz PM, King J, et al. Gene identification for ocular congenital cranial motor neuron disorders using human sequencing, zebrafish screening, and protein binding microarrays. *Invest Ophthalmol Vis Sci.* 2025;66(3):62. https://doi.org/10.1167/iovs.66.3.62

Purpose. To functionally evaluate novel human sequence-derived candidate genes and variants for unsolved ocular congenital cranial dysinnervation disorders (oCCDDs).

Methods. Through exome and genome sequencing of a genetically unsolved human oCCDD cohort, we previously reported the identification of variants in many candidate genes. Here, we describe a parallel study that prioritized a subset of these genes (43 human genes, 57 zebrafish genes) using a G0 CRISPR/Cas9-based knockout assay in zebrafish and generated F2 germline mutants for 17. We tested the functionality of variants of uncertain significance in known and novel candidate transcription factor-encoding genes through protein binding microarrays.

Results. We first demonstrated the feasibility of the G0 screen by targeting known oCCDD genes *phox2a* and *mafba*. Approximately 70% to 90% of gene-targeted G0 zebrafish embryos recapitulated germline homozygous null-equivalent phenotypes. Using this approach, we then identified three novel candidate oCCDD genes (*SEMA3F*, *OLIG2,* and *FRMD4B*) with putative contributions to human and zebrafish cranial motor development. In addition, protein binding microarrays demonstrated reduced or abolished DNA binding of human variants of uncertain significance in known and novel sequence-derived transcription factors *PHOX2A* (p.(Trp137Cys)), *MAFB* (p.(Glu223Lys)), and *OLIG2* (p.(Arg156Leu)).

Conclusions. This study nominates three strong novel candidate oCCDD genes (*SEMA3F*, *OLIG2,* and *FRMD4B*) and supports the functionality and putative pathogenicity of transcription factor candidate variants *PHOX2A* p.(Trp137Cys), *MAFB* p.(Glu223Lys), and *OLIG2* p.(Arg156Leu). Our findings support that G0 loss-of-function screening in zebrafish can be coupled with human sequence analysis and protein binding microarrays to aid in prioritizing oCCDD candidate genes/variants.

Keywords: congenital cranial dysinnervation disorder, cranial nerve, eye movement, zebrafish, incomitant strabismus

Human exome and genome sequencing have facilitated Mendelian gene discovery but generate numerous candidate genes and variants, only a subset of which are pathogenic. Moreover, heterogeneous loci and alleles hinder the identification of recurrently mutated genes or alleles. Targeted modeling can assess functionality but is often limited in throughput and applicability across disparate genes and phenotypes. This disconnect between candidate disease gene identification and functional validation remains a barrier to gene discovery for phenotypes including the ocular congenital cranial dysinnervation disorders (oCCDDs).

The oCCDDs are characterized by congenitally restricted eye or eyelid movement and result from maldevelopment of the oculomotor (CN3), trochlear (CN4), or abducens (CN6) motor neurons and axons (Figs. 1A, 1B). Some oCCDDs include congenital ptosis, Marcus Gunn jaw-winking syndrome (MGJWS), congenital fibrosis of the extraocular muscles (CFEOM), and Duane retraction syndrome (DRS). Congenital ptosis is characterized by eyelid drooping and can result from CN3 maldevelopment. In MGJWS, congenital ptosis transiently improves with specific jaw movements because of synkinetic miswiring by the motor trigeminal nerve (CN5). CFEOM results from maldevelopment of CN3 and in some cases also CN4 or CN6 and is typified by nonprogressive restriction of vertical eye movement with variable ptosis and variable restrictions of horizontal gaze. In DRS, CN6 maldevelopment causes limited abduction and variably limited adduction, and the globe retracts on attempted adduction because of synkinetic miswiring by CN3.

Some oCCDDs are caused by monoallelic or biallelic loss of function (LOF) of transcription factors. Biallelic *PHOX2A* LOF causes CFEOM in humans and absence of CN3/CN4 motor nuclei in mice.[1] Monoallelic *MAFB* LOF causes DRS in humans and absence of CN6 motor nuclei in mice, with secondary aberrant innervation by CN3 of the lateral rectus muscle, which is normally innervated by CN6.[2] Although these and other mechanisms explain some oCCDDs, many remain genetically undefined. We recently reported exome/genome sequencing of a large human oCCDD cohort, which yielded many candidate genes and variants of uncertain significance whose pathogenicity remain untested.[3]

Targeted in vitro or in vivo modeling can enhance functional understanding of candidate genes/variants. For instance, candidate variants in transcription factors can be assessed by universal protein binding microarrays, a high-throughput method that tests DNA binding capacity of wild-type or variant transcription factors.[4,5] Additionally, oCCDD genetics and pathophysiology can be elucidated with animal models including zebrafish (*Danio rerio*). Zebrafish have advantages over mammals, including fecundity and rapid external development.[6] Moreover, 69% of human genes and 82% of human disease-associated genes in Online Mendelian Inheritance in Man (OMIM)[7] have fish orthologs; some of these human genes are represented as duplicated paralogous genes in fish.[8] Zebrafish are amenable to gene editing and live imaging, and their ocular motor neurons are detected by 24 to 30 hours post-fertilization (hpf) and innervate their target muscles by 72 hpf.[9] Zebrafish lack eyelids and the CN3 branch that innervates them, but their cranial nerve anatomy and eye movements are otherwise conserved.[6,9]

Zebrafish ocular motor development has been characterized through transgenic reporters including a *Tg*(*isl1:GFP*) line labeling all cranial motor neurons and their axons except CN6,[10] and an HGj4A *mnr2b/hlxb9lb* enhancer trap line labeling CN6 motor neurons and axons (Fig. 1C).[11] As in mammals, *phox2a*$^{-/-}$ fish have absent or malformed CN3 and CN4 nuclei,[12–14] and *mafba*$^{-/-}$ fish have absent or hypoplastic CN6 nuclei.[15–17] Thus zebrafish are an excellent model for moderate-throughput testing of oCCDD candidate genes.

Standard homozygous null zebrafish are derived in the F2 generation and require six months to generate. Prior studies have expedited this timeline by generating G0 mutants using simultaneous injection of multiple high-dose CRISPR guide RNAs redundantly targeting one gene.[18–21] This approach is reported to reproduce homozygous null-equivalent phenotypes in >90% of embryos with <18% toxicity. Because the cranial motor system is conserved between zebrafish and humans and there are existing transgenic lines labeling the ocular cranial motor system, oCCDDs represent a unique model for testing the G0 knockout approach. Here we report the successes and limitations of functionally assessing human candidate oCCDD genes using moderate-throughput CRISPR/Cas9 G0 LOF screening in zebrafish, and testing functionality of transcription factor candidate variants by protein binding microarrays (Fig. 1D).

Methods

Additional details for the following sections are provided in Supplementary Methods.

Human Consenting and Phenotyping

Our study was approved by the Boston Children's Hospital (BCH) Institutional Review Board (IRB 05-03-036R) and complied with ethical recommendations of BCH and the Declaration of Helsinki. Research participants or legal guardians provided written informed consent. Phenotypes were obtained from review of clinical records and from

A **Human ocular and trigeminal motor nerves**

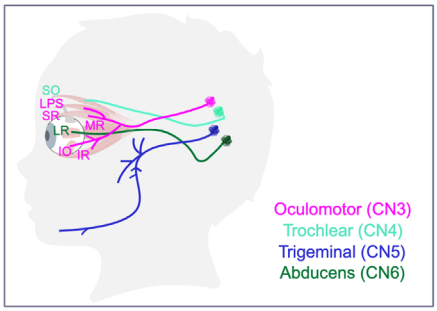

B **CN involvement in oCCDDs and zebrafish lines used to screen for phenotypes**

	CFEOM	Congenital ptosis	MGJWS	DRS
CN3	+, defective innervation of CN3 target muscle(s)	+, defective innervation of the LPS muscle	+, defective innervation of the LPS muscle	+, aberrant innervation of the LR muscle
CN4	+/-, defective SO muscle innervation in some forms of CFEOM	-	-	-
CN5	-	-	+, aberrant innervation of the LPS muscle	-
CN6	+/-, hypoplasia in some forms of CFEOM	-	-	+, defective innervation of the LR muscle
Zebrafish line	*Tg(Isl1:GFP)*	*Tg(Isl1:GFP)*	*Tg(Isl1:GFP)*	*HGj4A mnr2b/hlxb9lb*

C **Zebrafish ocular and trigeminal motor nerves (72 hpf)**

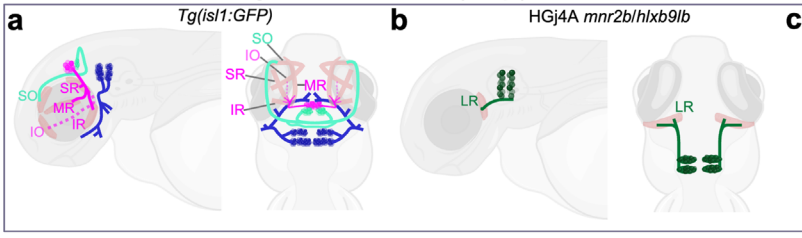

c

oCCDD-relevant CNs	Present in zebrafish?	Labeled by *Tg(isl1:GFP)* line?	Labeled by HGj4A line?
Oculomotor (CN3)			
IO branch	Yes	No	No
IR branch	Yes	Yes	No
LPS branch	No	No	No
MR branch	Yes	Yes	No
SR branch	Yes	Yes	No
Trochlear (CN4)	Yes	Yes	No
Trigeminal (CN5)	Yes	Yes	No
Abducens (CN6)	Yes	No	Yes

D **Workflow for identification and screening of known and novel oCCDD candidate genes/variants**

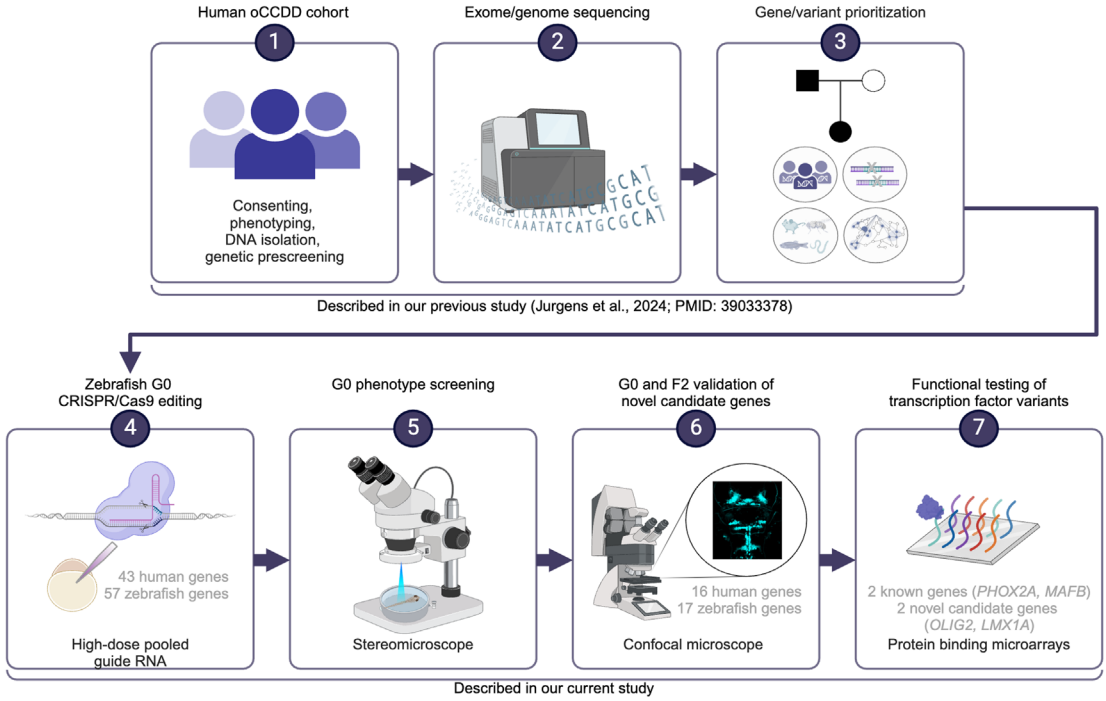

E **Demographics of 46 sequenced human probands whose 43 distinct candidate genes were tested in the zebrafish screen**

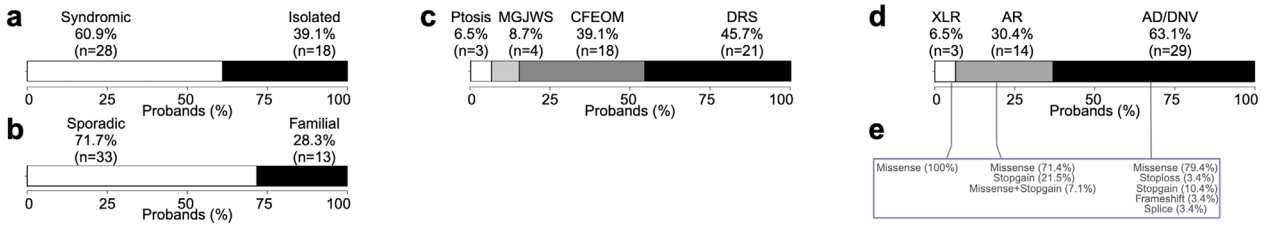

Figure 1. Human and zebrafish cranial motor nerves and study workflow. (**A**) In the human brainstem, motor neurons cluster into cranial motor nuclei, whose axons form the CNs. The oCCDDs can arise from defective formation, identity, and/or axonal projections of three of these motor neuron populations (CN3, CN4, and CN6) that collectively innervate seven extraocular muscles to orchestrate eye/eyelid movement. CN3 innervates the IO, IR, LPS, MR, and SR muscles. CN4 innervates the SO muscle, and CN6 innervates the LR muscle. CN5 normally innervates the muscles of mastication (not shown) but can also aberrantly innervate the LPS muscle in MGJWS. (**B**) Summary of CN pathology in humans or mice with specific oCCDDs, and the zebrafish reporter lines used to analyze them. To model oCCDDs in zebrafish, our study leveraged the HGj4A *mnr2b/hlxb9lb* line for DRS candidate genes and the *Tg(isl1:GFP)* line for CFEOM, congenital ptosis, and

MGJWS genes. (**C**) Zebrafish wild-type ocular and trigeminal motor nerves visualized in the *Tg(isl1:GFP)* (**a**) or HGj4A reporter line (**b**). Left-lateral view; right-dorsal view. (**c**) Summary of oCCDD-relevant CNs that are present in zebrafish and labeled by each reporter line. (**a**, **c**) As in humans, zebrafish CN3 innervates the IO, IR, MR, and SR muscles. However, the CN3 branch to the IO muscle cannot be visualized with the *Tg(isl1:GFP)* transgenic line. Additionally, unlike humans, zebrafish lack the LPS muscle and its corresponding CN3 subdivision. Zebrafish have bilateral CN4 motor nuclei and nerves (*left* and *right*). CN4 exits the brainstem dorsally and travels ventrally to innervate the contralateral SO muscle. At 72 hpf, wild-type zebrafish CN4 is variably defasciculated. Zebrafish have anterior and posterior trigeminal motor nuclei bilaterally, which extend axons for the motor trigeminal (CN5) nerve that innervates the muscles of mastication (not shown). (**b**, **c**) The HGj4A line labels the CN6 motor neurons and their axons. Zebrafish have anterior and posterior CN6 motor nuclei bilaterally, which extend CN6 nerves that target the LR muscles. (**D**) Workflow for the identification and screening of known and novel oCCDD candidate genes and variants. We reported steps 1-3 in our previous study describing exome/genome sequencing of our human oCCDD cohort[3] and performed steps 4–7 in the present study. (**E**) Demographics of the 46 human probands whose 43 distinct human candidate genes were tested in the zebrafish screen. Percentages of probands are shown with oCCDDs that are (**a**) syndromic or isolated, (**b**) sporadic or familial, (**c**) fitting various oCCDD subdiagnoses, or (**d**) fitting various modes of inheritance. (**e**) The types of variants fitting modes of inheritance defined in d are provided. AD, autosomal dominant; AR, autosomal recessive; CFEOM, congenital fibrosis of the extraocular muscles; CN, cranial nerve; CN3, oculomotor/cranial nerve 3; CN4, trochlear/cranial nerve 4; CN5, trigeminal motor/cranial nerve 5; CN6, abducens/cranial nerve 6; DNV, de novo variant; DRS, Duane retraction syndrome; hpf, hours post-fertilization; IO, inferior oblique muscle; IR, inferior rectus muscle; LPS, levator palpebrae superioris muscle; LR, lateral rectus muscle; MGJWS, Marcus Gunn jaw-winking syndrome; MR, medial rectus muscle; oCCDD, ocular congenital cranial dysinnervation disorder; Ptosis, congenital ptosis; SO, superior oblique muscle; SR, superior rectus muscle; XLR, X-linked recessive. *Pink*, CN3; *light green*, CN4; *dark blue*, CN5; *dark green*, CN6; *partially transparent brown*, extraocular muscle; *dashed line*, nerve that is present in zebrafish but not labeled with the transgenic reporter line.

participant questionnaires and updates. Clinically acquired brain magnetic resonance imaging (MRI) scans were reviewed retrospectively.

Prioritization, Cosegregation Analysis, and Classification of Human Sequence–Derived Alleles for Screening in Zebrafish

In our previously reported human oCCDD study, which was performed in parallel with the current zebrafish study, we leveraged human genetics to identify novel oCCDD candidate genes/variants through phenotyping and exome/genome sequencing of a large cohort of human pedigrees with oCCDDs.[3] In the current study, we used these human sequence–derived variants to prioritize candidate genes for the zebrafish screen based on conservation in zebrafish, recessive inheritance, novelty to oCCDD phenotype association, and/or predicted LOF of variants (Fig. 1D, Supplementary Table S1). Of the 43 human genes we prioritized for the zebrafish screen, 14 were among the 80 genes prioritized and highlighted in the previously reported study, whereas 29 human genes were identified but were not highlighted.[3] Sanger validation and familial cosegregation analysis are shown for candidate variants in genes that (1) yielded cranial motor phenotypes in both G0 and F2 mutants in our zebrafish screen and/or (2) encoded transcription factors tested by protein binding microarray (Supplementary Table S2). Variants were classified using criteria from the American College of Genetics and Genomics and Association for Molecular Pathology[22] and the Clinical Genome Resource[23] (Supplementary Methods).

G0 Screening and F2 Germline Validation in LOF Zebrafish Models of Prioritized Genes

Zebrafish studies were conducted in accordance with the ARVO Statement for the Use of Animals in Ophthalmic and Vision Research. G0 targeting experiments consisted of microinjecting single cell-stage embryos with four high-dose (1 ug/uL) guide RNAs redundantly targeting each gene at multiple sites predicted to result in nonsense-mediated decay, with the goal to generate full-gene knockouts.[20] When available, guide RNAs were selected that each targeted separate exons to increase the probability of full-gene knockout for multiple isoforms. In most cases of human gene duplication in zebrafish, we targeted each paralog through an independent G0 targeting experiment. Exceptions to this were as follows: (a) For the *MAFB* human gene, only the *mafba* fish gene was targeted because this zebrafish gene had been demonstrated to have CN6 maldevelopment in germline knockout models,[24] and because targeting of this gene was intended to be a proof-of-principle of G0 targeting efficacy. (b) For the *HOXA10* human gene, one of the duplicated zebrafish genes encodes a pseudogene, so only the non-pseudogene paralog was targeted. (c) For the *FOXG1, ARX*, and *SCN1A* human genes, only the most conserved paralog was targeted because of pandemic-related restrictions in fish facility access. At 72 hpf, injected G0 fish were assessed by stereomicroscope for gross phenotypic changes in cranial motor neuron nuclei and/or nerves. For genes whose targeting induced putative phenotypes in at least a subset of injected fish, we performed two additional G0 experimental replicates and F2 germline mutant validation and visualized with confocal imaging (Fig. 1D).

Protein Structural Mapping and Universal Protein Binding Microarray Testing of Transcription Factor Candidate Variants

Two-dimensional protein structural maps were generated for genes/variants validated through the zebrafish screen and/or protein binding microarrays along with previously reported oCCDD-associated variants (Supplementary Methods). Protein binding microarrays were used to assess DNA binding capabilities and predicted motif logos for variants of uncertain significance in the DNA binding domains of known (*PHOX2A, MAFB*) or novel (*OLIG2, LMX1A*) transcription factor-encoding candidate genes relative to their wild-type counterparts (Fig. 1D; Supplementary Methods).[5,25] See Supplementary Methods for protein binding microarray variant selection criteria.

Results

Prioritization of Human Sequence–Derived oCCDD Candidate Genes for Screening in Zebrafish

For G0 LOF targeting and anatomic screening in zebrafish, we chose 43 human candidate genes among 46 probands

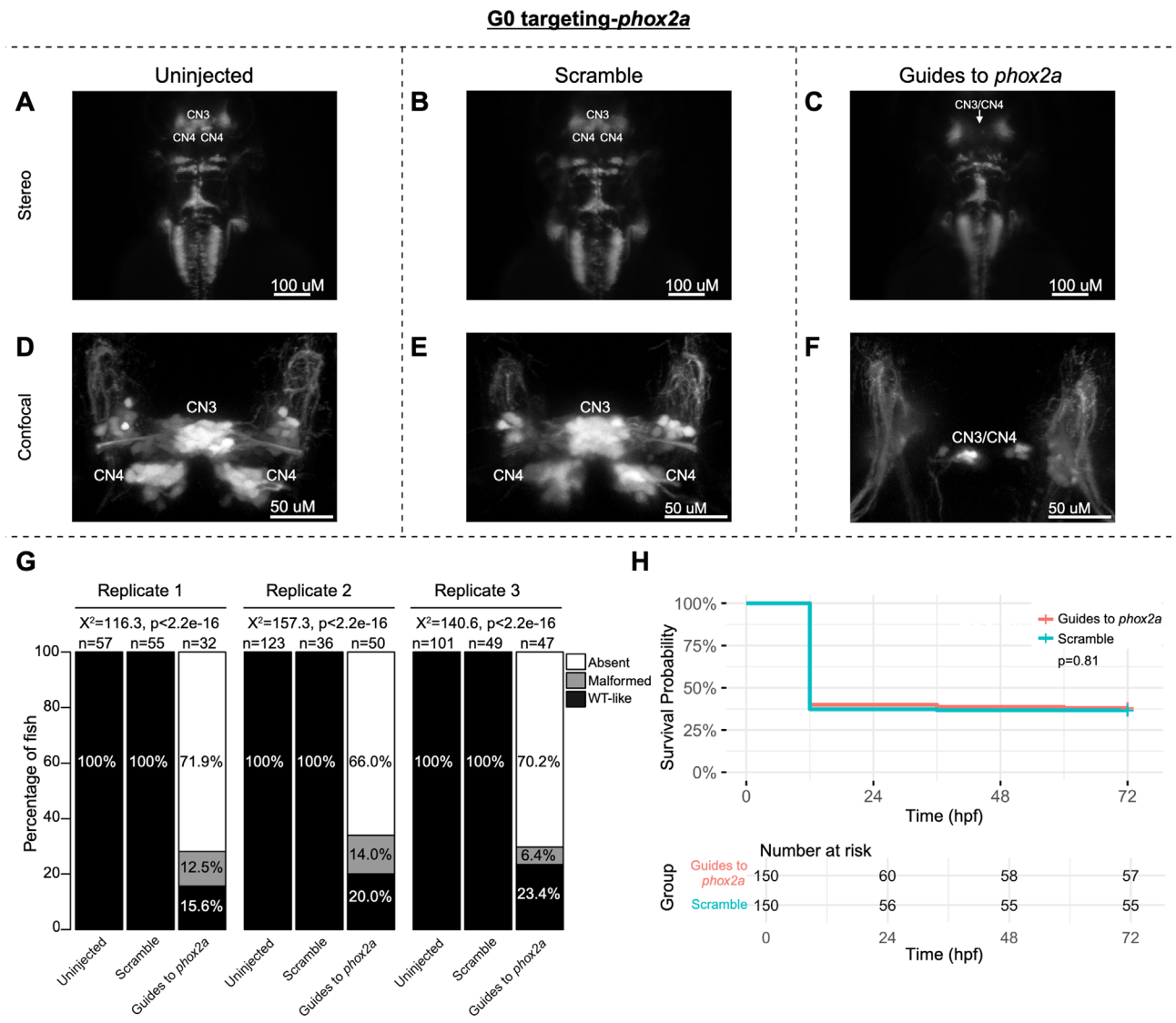

Figure 2. G0 zebrafish targeting of *phox2a*. Representative images obtained by stereomicroscope (**A**–**C**) and confocal microscopy (**D**–**F**) of uninjected (**A**, **D**), scramble-injected (**B**, **E**), or *phox2a*-targeting guide-injected G0 *Tg(isl1:GFP)* zebrafish at 72 hpf. Stereomicroscope images for each treatment group correspond to the confocal images obtained from the same fish in the panel below. Because residual motor neurons from CN3 and/or CN4 could not be definitively assigned to either of these specific motor neuron nuclei, CN3/CN4 were labeled as a single entity in Guide-targeted fish. Note apparent absence (**C**) or paucity (**F**) of CN3/CN4 motor neurons following *phox2a* G0 mosaic knockout. (**G**) Barplots showing the percentages of zebrafish exhibiting wild-type-like ("WT-like"), malformed, or absent CN3/CN4 motor nuclei, as scored under the dissecting stereomicroscope in G0 zebrafish at 72 hpf. Total numbers of fish in each group are given above the corresponding bar. Data are shown from three experimental replicates. Pearson's 3 × 3 χ^2 test with 4 degrees of freedom; *P* values and χ^2 values provided for each replicate. (**H**) Kaplan-Meier survival curves demonstrating the relative survival probabilities of scramble-injected (*blue line*) and guide-injected (*pink line*) zebrafish over the first 72 hours of life. "Number at risk" below the plot provides the counts of surviving embryos in each group taken every 24 hpf over a 72 hpf period. Relative survival probabilities of *phox2a*-targeting and scrambled gRNA-injected embryos were compared by the log-rank test. Displayed data were derived from a single experimental replicate, but measurements were taken for three experimental replicates, all of which showed the same trend.

from our previously reported analysis of exome/genome sequences of 467 oCCDD pedigrees (Fig. 1D).[3] Three of the 43 genes had rare variants of interest in two probands (*ACTR1B, KCNAB1, FOXC1;* Fig. 1D, Supplementary Table S1), two had well established roles in oCCDDs before this study (*PHOX2A, MAFB*), and four had only occasional reported association with human oCCDDs (*ARX, COL25A1, DYRK1A, KIFBP*). Thirty-seven were novel oCCDD candidates, seven of which were highlighted in our previous report.[3]

Summaries of the oCCDDs, modes of inheritance, and nature of the candidate variants in these 46 probands are provided (Fig. 1E). Probands predominantly had syndromic (60.9%) and sporadic (71.7%) oCCDDs, most of which were DRS (45.7%) or CFEOM (39.1%). Most candidate variants were identified under autosomal dominant/de novo models (63.1%), and most were missense (78.3% across all inheritance models) with fewer putative LOF variants (21.7%).

The zebrafish orthologs of these 43 human genes were subjected to a G0 CRISPR/Cas9 editing pipeline in zebrafish. Fourteen of the human genes had two highly homologous zebrafish paralogs (*CELF5, DBX1, DYRK1A, FOXC1, FRMD4B, MXRA8, NAV2, NTN1, PPP1R14B, SDK1,*

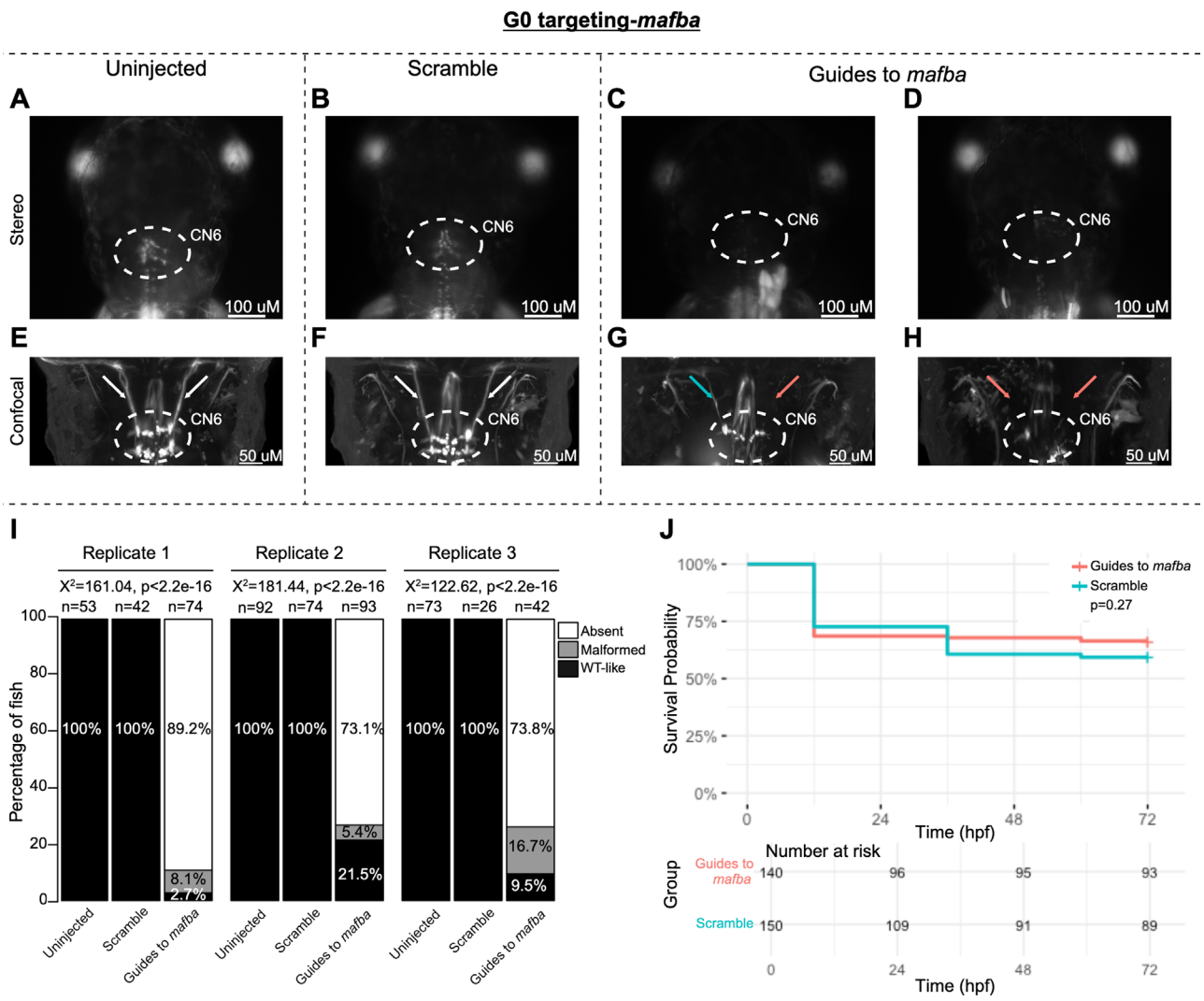

Figure 3. G0 zebrafish targeting of *mafba*. (**A–H**) Representative images obtained by stereomicroscope (**A–D**) and confocal microscopy (**E–H**) of uninjected (**A**, **E**), scrambled guide-injected (**B**, **F**), or *mafba*-targeting guide-injected (**C**, **D**, **G**, **H**) G0 HGj4A zebrafish at 72 hpf. Two images are provided for guide-injected fish, demonstrating variability in G0 targeting outcomes. Stereomicroscope images for each treatment group correspond to the confocal images obtained from the same fish in the panel below. Motor neurons in the abducens nucleus (*dashed white circled region*) appear absent by stereomicroscopy (**C**, **D**) or variably reduced (**G**, **H**) by confocal microscopy, and abducens nerves appear thin (**G;** *blue arrow*) or absent (**G**, **H;** *red arrows*) compared to normal (**E**, **F**; *white arrows)* by confocal microscopy. (**I**) *Bar plots* showing the percentages of zebrafish exhibiting wild-type-like (*WT-like*), malformed, or absent CN6 motor neuron nuclei, as scored under the dissecting stereomicroscope in G0 zebrafish at 72 hpf. Total numbers of fish in each group are given above the corresponding bar. Data are shown from three experimental replicates. Pearson's 3 × 3 χ^2 test with 4 degrees of freedom; *P* values and χ^2 values provided for each replicate. (**J**) Kaplan-Meier survival curves demonstrating the relative survival probabilities of scramble-injected (*blue line*) and guide-injected (*pink line*) zebrafish over the first 72 hours of life. *Number at risk* below the plot provides the counts of surviving embryos in each group taken every 24 hpf over a 72 hpf period. Relative survival probabilities of *mafba*-targeting guide-injected and scrambled-injected embryos were compared by the log-rank test. Displayed data were derived from a single experimental replicate, but measurements were taken for three experimental replicates, all of which showed the same trend.

SEMA3F, SEMA5B, SLC12A5, TLE3), and thus 57 zebrafish genes were targeted. Each zebrafish paralog was targeted independently.

G0 Screen and F2 Zebrafish Modeling for Human Sequence–Derived oCCDD Candidate Genes

To pilot the G0 LOF zebrafish assay, we targeted the known oCCDD genes *phox2a* and *mafba* (Figs. 2, 3). G0 targeting of both genes recapitulated known germline LOF phenotypes. G0-targeted fish had grossly absent (*phox2a:* 69.0%, *mafba:* 78.9%) or malformed (*phox2a*: 10.9%, *mafba*: 8.6%) CN3/CN4 or CN6 motor neuron nuclei, respectively, with absence or thinning of the corresponding cranial nerves (Figs. 2A–G, Figs. 3A–I). Targeting of each gene had no significant impact on survival (Fig. 2H, Fig. 3J).

Encouraged by these results, we performed G0 targeting of the remaining 55 zebrafish oCCDD candidate genes (41 human genes; Supplementary Table S1). These included 32 zebrafish candidate genes (23 human genes, nine of which were duplicated in fish) for CFEOM, ptosis, or MGJWS and 23 zebrafish candidate genes (18 human genes, five of which

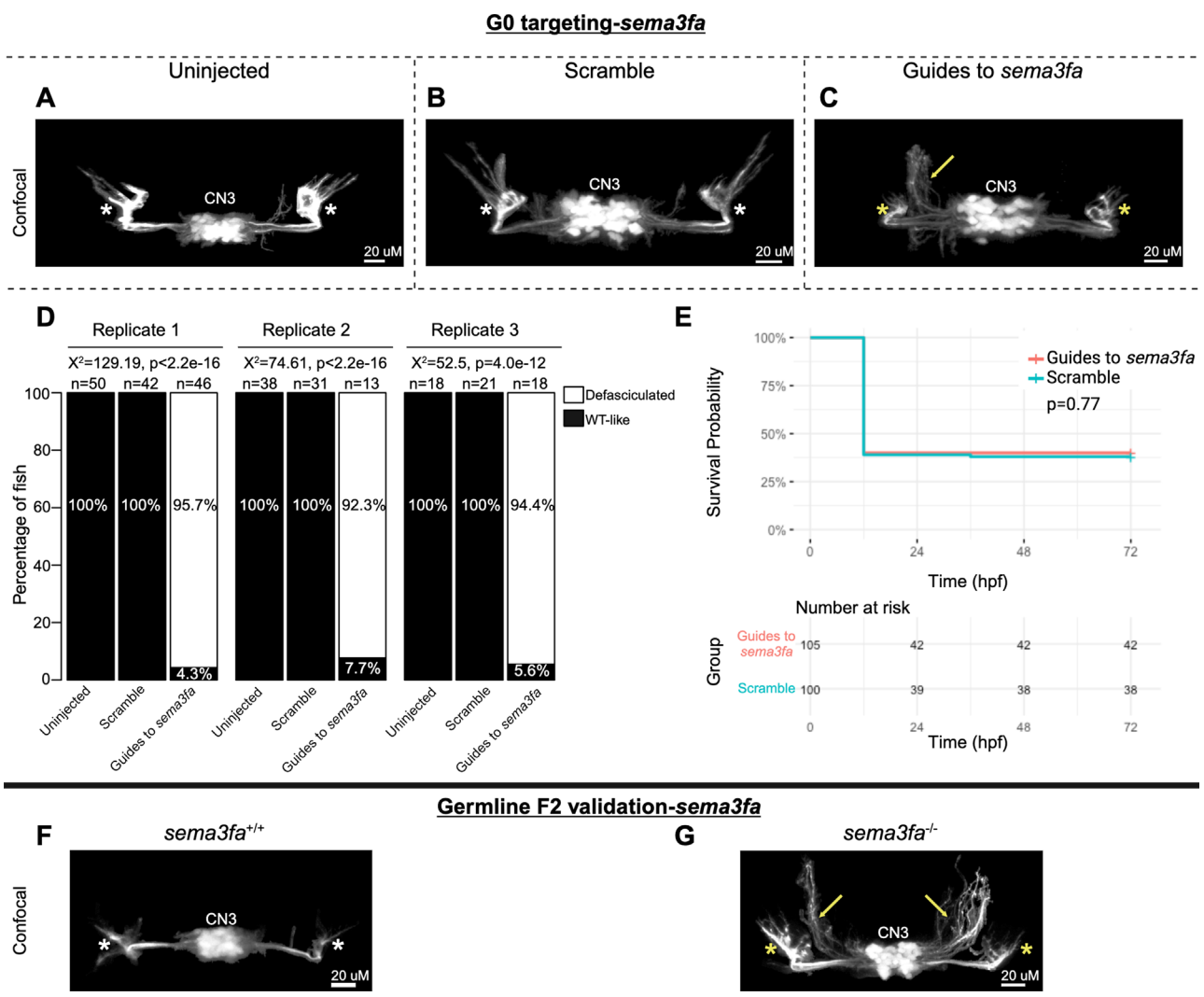

Figure 4. G0 mosaic and F2 germline zebrafish targeting of *sema3fa*. (**A–E**) Initial *sema3fa* targeting experiments were performed in G0 embryos. Representative images obtained by confocal microscopy (**A–C**) of uninjected (**A**), scrambled guide-injected (**B**), or *sema3fa*-targeting guide-injected (**C**) G0 *Tg(isl1:GFP)* zebrafish at 72 hpf. Note defasciculated CN3 (*yellow arrow*) and failed CN3 nerve extension toward extraocular muscles (*yellow stars*) relative to uninjected and scramble-injected CN3 (*white stars*). CN3, cranial nerve 3 (oculomotor); *yellow arrow*, increased defasciculation of CN3 nerve; *yellow star*, failed extension of CN3 nerve toward target extraocular muscles; *white star*, typical CN3 branches toward extraocular muscles. (**D**) *Bar plots* showing the percentages of zebrafish exhibiting wild-type-like (*WT-like*) or defasciculated CN3 nerve(s), as scored under the dissecting stereomicroscope in G0 zebrafish at 72 hpf. Total numbers of fish in each group are given above the corresponding bar. Data are shown from three experimental replicates. Pearson's 2×3 χ^2 test with 2 degrees of freedom; for each of three experimental replicates, $\chi^2 = 129.19$, $P < 2.2e^{-16}$; $\chi^2 = 74.61$, $P < 2.2e^{-16}$; $\chi^2 = 52.5$, $P = 4.0e^{-12}$. (**E**) Kaplan-Meier survival curves demonstrating the relative survival probabilities of scramble-injected (*blue line*) and guide-injected (*pink line*) zebrafish over the first 72 hours of life. *Number at risk* below the plot provides the counts of surviving embryos in each group taken every 24 hpf over a 72 hpf period. Relative survival probabilities of *sema3fa*-targeting and scrambled gRNA-injected embryos were compared by the log-rank test. Displayed data were derived from a single experimental replicate, but measurements were taken for three experimental replicates, all of which showed the same trend. (**F**, **G**) Representative images from wild-type or F2 germline *sema3fa*$^{-/-}$ (c.869_873delTGAGA, p.(Glu290GlyfsTer8)) mutants (*arrows* and *stars* as per **A–C**).

were duplicated in fish) for DRS. In preliminary results from one pilot injection experiment per gene, G0 mutants for 17 novel zebrafish candidate oCCDD genes (16 human genes) appeared to have at least mild malformation of cranial motor nuclei/nerves in at least a subset of G0 embryos visualized by stereomicroscope (Supplementary Table S4). The ocular cranial nerve anatomy of these 17 fish were then examined at higher resolution with confocal microscopy of additional G0 targeting replicates and F2 germline mutants. The oCCDD phenotype was confirmed in three putative novel oCCDD candidate genes: *sema3fa, olig2,* and *frmd4bb* (Figs. 4–6, respectively; Supplementary Figs. S1, S2).

In G0 *sema3fa* mosaic null mutants, CN3 nuclei were present and appeared grossly intact. However, CN3 axons had increased defasciculation in 94.8% of fish and failed to project to their target extraocular muscles (Figs. 4A–D). There was a statistically significant association between treatment group and the proportions of fish with CN3 defasciculation but no statistically significant difference in survival (Figs. 4D, 4E). Under the stereomicroscope, axonal defasciculation was visible but poorly resolved and

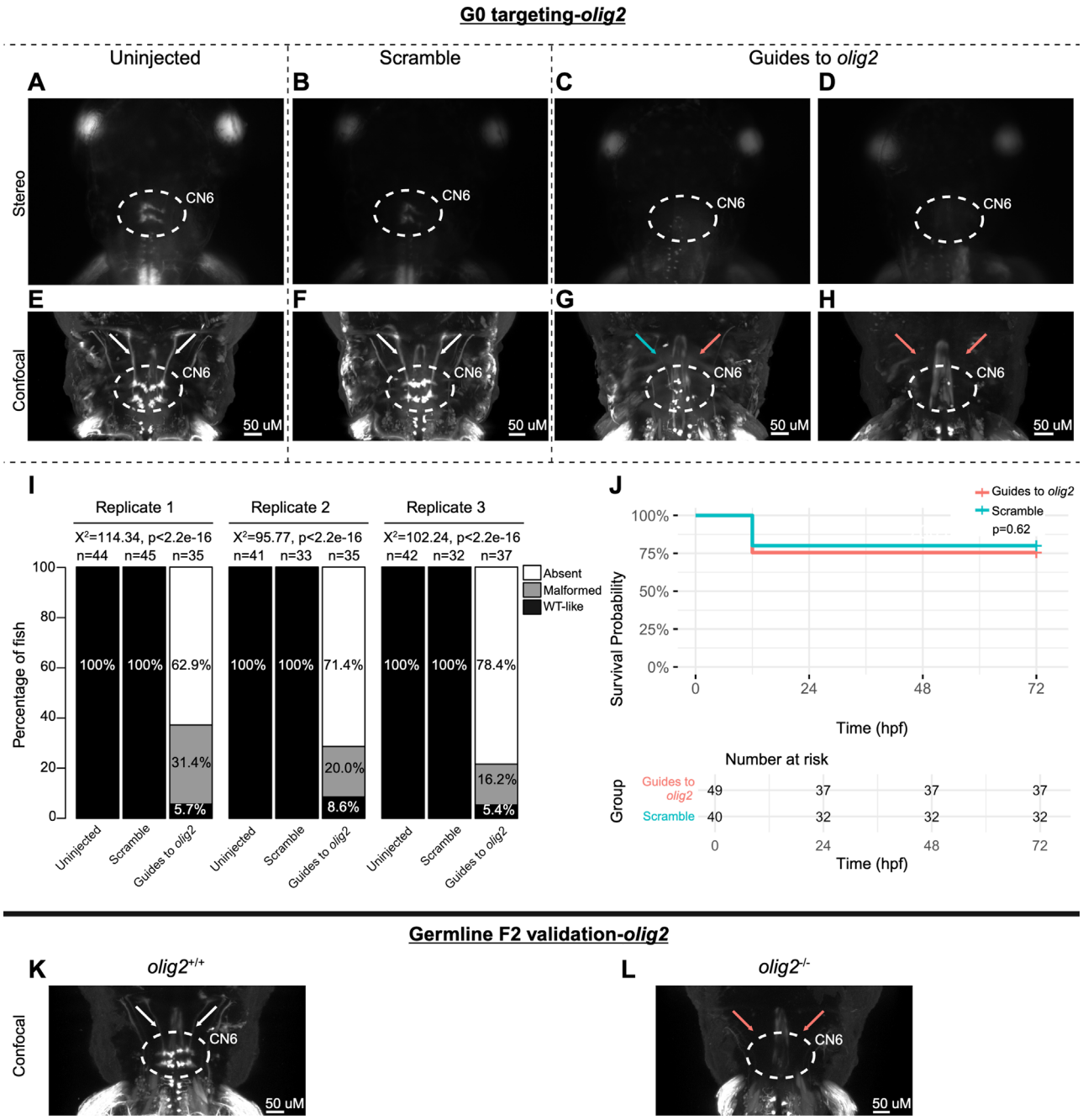

Figure 5. G0 mosaic and F2 germline zebrafish targeting of *olig2*. (**A–H**) Initial *olig2* targeting experiments were performed in G0 embryos. Representative images obtained by stereomicroscope (**A–D**) and confocal microscopy (**E–H**) for Uninjected (**A**, **E**), Scrambled guide injected (**B**, **F**), or *olig2*-targeting Guide-injected (**C–D**, **G–H**) G0 HGj4A zebrafish at 72 hpf. Two images are provided for guide-injected fish, to demonstrate variability in G0 targeting outcomes. Stereomicroscope images for each treatment group correspond to the confocal images obtained from the same fish in the panel below. Motor neurons in the abducens nucleus (*dashed white circled region*) appear absent by stereomicroscopy (**C**, **D**) or variably reduced (**G**, **H**) by confocal microscopy, and abducens nerves appear thin (**G**; *blue arrow*) or absent (**G**, **H**; *red arrows*) compared to normal (**E**, **F**; *white arrows*) by confocal microscopy. (**I**) *Bar plots* showing the percentages of zebrafish exhibiting wild-type-like (*WT-like*), malformed, or absent CN6 motor neuron nuclei, as scored under the dissecting stereomicroscope in G0 zebrafish at 72 hpf. Total numbers of fish in each group are given above the corresponding bar. Data are shown from three experimental replicates. Pearson's 3×3 χ^2 test with 4 degrees of freedom; $\chi^2 = 114.34, 95.77, 102.24$ for each of three experimental replicates; $P < 2.2e^{-16}$. (**J**) Kaplan-Meier survival curves demonstrating the relative survival probabilities of scramble-injected (*blue line*) and guide-injected (*pink line*) zebrafish over the first 72 hours of life. *Number at risk* below the plot provides counts of surviving embryos in each group taken every 24 hpf over a 72 hpf period. Relative survival probabilities of *olig2*-targeting and scrambled gRNA-injected embryos were compared by the log-rank test. Displayed data were derived from a single experimental replicate, but measurements were taken for three experimental replicates, all of which showed the same trend. (**K**, **L**) Representative images from wild-type or F2 germline *olig2*$^{-/-}$ mutants (c.496_499delAGTT, p.(Ser166ValfsTer93)); key as noted for **A–H**).

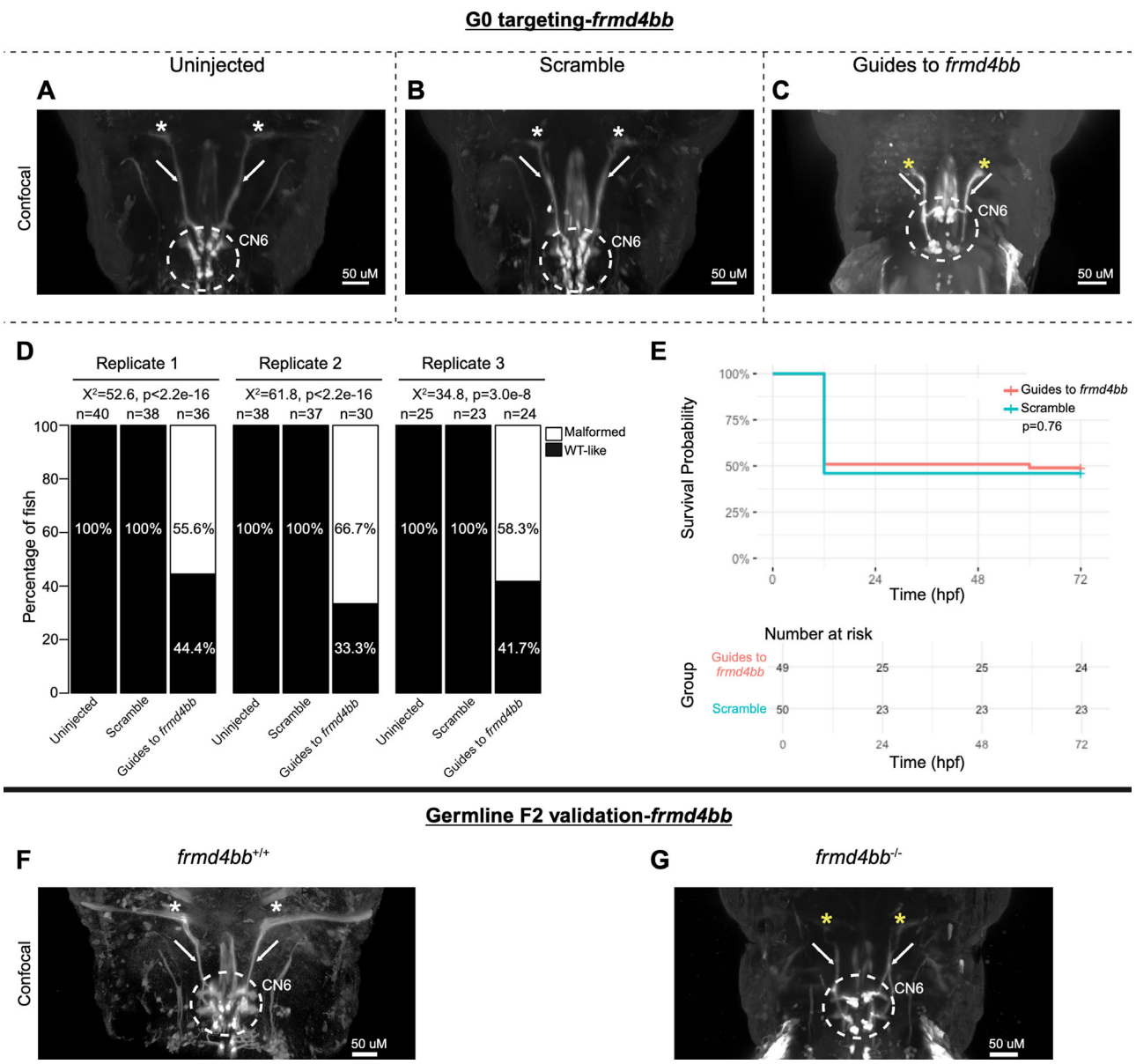

Figure 6. G0 mosaic and F2 germline zebrafish targeting of *frmd4bb*. (**A–E**) Initial *frmd4bb* targeting experiments were performed in G0 embryos. Representative images obtained by confocal microscopy (**A–C**) of uninjected (**A**), scrambled guide-injected (**B**), or *frmd4bb*-targeting guide-injected (**C**) G0 HGj4A zebrafish at 72 hpf. Motor neurons in the abducens nucleus (*dashed white circled region*) have reduced dispersion through the columns of the abducens nuclei (**C**), and abducens nerves appear stalled and fail to target the lateral rectus muscles (**C;** *white arrows* and *yellow stars*) compared to uninjected and scrambled (**A**, **B;** *white arrows* and *white stars*). (**D**) *Bar plots* showing the percentages of zebrafish exhibiting wild-type-like (*WT-like*) or malformed CN6 motor neuron nuclei, as scored under the dissecting stereomicroscope in G0 zebrafish at 72 hpf. Total numbers of fish in each group are given above the corresponding bar. Data are shown from three experimental replicates. Pearson's 2×3 χ^2 test with 2 degrees of freedom; for each of three experimental replicates, $\chi^2 = 52.6$, $P < 2.2e^{-16}$; $\chi^2 = 61.8$, $p < 2.2e^{-16}$; $\chi^2 = 34.8$, $P = 3.0e^{-8}$. (**E**) Kaplan-Meier survival curves demonstrating the relative survival probabilities of scramble-injected (*blue line*) and guide-injected (*pink line*) zebrafish over the first 72 hours of life. *Number at risk* below the plot provides counts of surviving embryos in each group taken every 24 hpf over a 72 hpf period. Relative survival probabilities of *frmd4bb*-targeting and scrambled gRNA-injected embryos were compared by the log-rank test. Displayed data were derived from a single experimental replicate, but measurements were taken for three experimental replicates, all of which showed the same trend. (**F**, **G**) Representative images from wild-type or F2 germline *frmd4bb*$^{-/-}$ mutants (c.1687_1697delGATGAAATGAA, p.(Asp563ProfsTer25)).

required manual focus adjustment through z-planes to visualize by eye. This was poorly captured by stereomicroscope imaging of a single z-plane (Supplementary Fig. S3A). F2 germline *sema3fa*$^{-/-}$ mutants (c.869_873delTGAGA, p.(Glu290GlyfsTer8)) also had increased CN3 defasciculation and failed extension toward CN3 target extraocular muscles relative to *sema3fa*$^{+/+}$ fish (Figs. 4F, 4G).

G0 *olig2* mutants had grossly absent (71.0%) or severely malformed (22.4%) CN6 nuclei with few residual motor neurons and absence or thinning of the CN6 nerves, reminiscent of *mafba*-null mutants (Figs. 5A–I). There was a statistically significant association between treatment group and the proportions of fish with each CN6 phenotype, but no statistically significant difference in

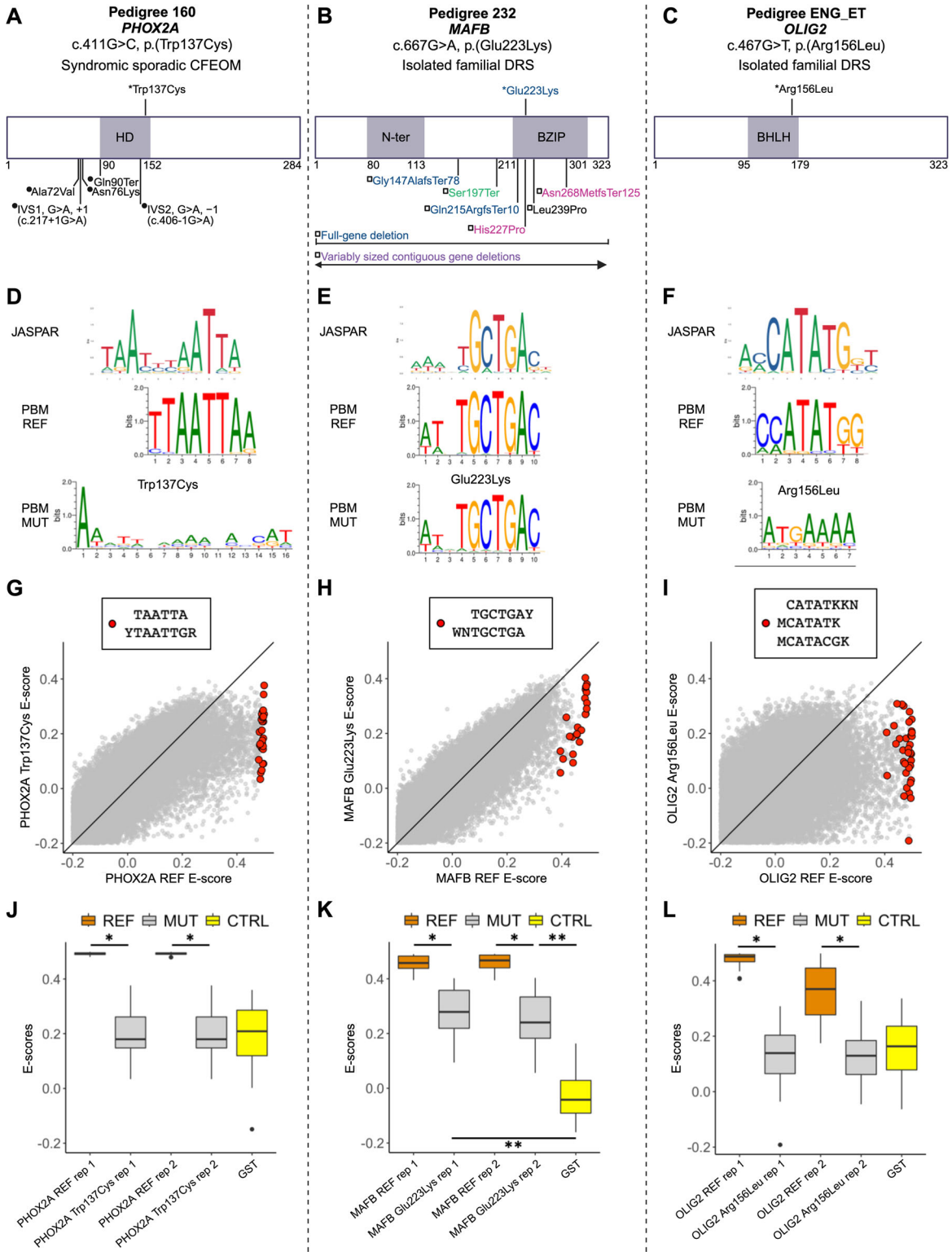

Figure 7. The oCCDD proband-derived candidate variants in transcription factors disrupt DNA binding. (**A–C**) Two-dimensional structural mapping of human variants. (**A**) Variants in PHOX2A associated with CFEOM. (**B**) Variants in MAFB associated with DRS and/or co-occurring phenotypes. (**C**) Variant in OLIG2 associated with DRS. References for Figure 7 are provided in Supplementary Methods and Results. *Asterisks* represent variants above schematics that were identified and reported in our sequenced human oCCDD cohort[1] and are functionally tested for the first time in this work: PHOX2A p.(Trp137Cys), MAFB p.(Glu223Lys), and OLIG2 p.(Arg156Leu). Variants below schematics are previously reported as follows: (**A**) *Filled circles* represent previously reported PHOX2A variants associated with CFEOM: IVS1, G>A, +1 (c.217+1G>A)[2]; IVS2, G>A, −1(c.406-1G>A)[2,3]; p.(Ala72Val)[2,3]; p.(Asn76Lys)[4]; p.(Gln90Ter).[5] (**B**) -Previously reported MAFB variants associated with DRS and colored as follows: *blue* denotes isolated DRS[6]; *magenta* denotes DRS ± hearing impairment ± intellectual disability[6,7]; *black* denotes DRS + focal segmental glomerulosclerosis ± hearing impairment[8]; *green* denotes focal segmental glomerulosclerosis

± DRS[9]; *purple* denotes contiguous gene deletions with variable neurodevelopmental anomalies ± DRS.[10] Variants are mapped using the following transcripts: ENST00000298231.5 (PHOX2A), ENST00000373313.3 (MAFB), and ENST00000382357.4 (OLIG2). (**D–F**) Transcription factor binding site motif logos for PHOX2A (**D**), MAFB (**E**), and OLIG2 (**F**). *Top*: logos from the JASPAR database of transcription factor binding profiles derived from high-throughput sequencing SELEX (HT-SELEX) experiments for either the wild-type human protein (PHOX2A and OLIG2) or orthologous mouse protein (Mafb). *Middle* and *bottom*: Protein binding microarray (PBM) experiment motifs derived from universal protein binding microarrays for the reference DNA binding domain (PBM REF, middle) and for the mutant DNA binding domain (PBM MUT, bottom). (**G–I**) For 8-mers resembling the wild-type motif, E-score comparison between reference and mutant DNA binding domain for PHOX2A (G), MAFB (H), and OLIG2 (I). Red dots correspond to 8-mer sequences that contain the labeled International Union of Pure and Applied Chemistry code-based *k*-mers, which are selected to closely resemble each motif logo. *Y*, C or T nucleotides; *R*, A or G nucleotides; *W*, A or T nucleotides; *M*, A or C nucleotides; *K*, G or T nucleotides; *N*, any base. (**J–L**) The 8-mer E-score comparison for the *k*-mers labeled in **G–I** across the replicate protein binding microarrays. (**J**) Reference versus p.(Trp137Cys) PHOX2A variant. PHOX2A p.(Trp137Cys) led to a significant drop in E-scores for 8-mers resembling the wild-type motif ($P < 10^{-9}$; one-sided Mann-Whitney U test) to a level indistinguishable from E-scores of the GST negative control ($P > 0.9$; two-sided Mann-Whitney U test). (**K**) Reference versus p.(Glu223Lys) MAFB variant. The E-scores for the 8-mers recognized by the wild-type MAFB showed significantly lower values for the mutant DNA binding domain ($P < 10^{-7}$; one-sided Mann-Whitney U test), but the E-score distribution for the mutant was still higher than that of the GST-negative control ($P < 10^{-6}$; two-sided Mann-Whitney U test), suggesting partial loss of binding. (**L**) Reference versus p.(Arg156Leu) OLIG2 variant. OLIG2 p.(Arg156Leu) led to a significant reduction in mutant E-scores for 8-mers recognized by wild-type OLIG2 ($P < 10^{-10}$; one-sided Mann-Whitney U test) to a level similar to that of the GST-tagged negative control ($P > 0.1$; two-sided Mann-Whitney U test). *Orange*, reference protein; *gray*, mutant/nonreference protein; *yellow*, GST-tagged negative control. * $P < 1 \times 10^{-7}$; one-sided Mann-Whitney U test. ** $P < 1 \times 10^{-6}$; two-sided Mann-Whitney U test. BHLH, basic helix-loop-helix domain; BZIP, basic leucine zipper domain; CFEOM, congenital fibrosis of the extraocular muscles; CTRL, GST-negative control protein; DRS, Duane retraction syndrome; *GS*, glutathione S-transferase tagged negative control protein; HD, homeodomain; MUT, mutant/nonreference; N-ter, N-terminal region; PBM, protein-binding microarray; REF, reference (nonmutant) sequence; rep, replicate.

survival (Figs. 5I, 5J). Like G0 mutants, F2 germline *olig2*$^{-/-}$ mutants (c.496_499delAGTT, p.(Ser166ValfsTer93)) had grossly absent or malformed CN6 motor neuron nuclei with absent or thin CN6 nerves (Figs. 5K, 5L).

Finally, CN6 nuclei were universally present but malformed in 60.0% of *frmd4bb*-targeted G0 mutants, with reduced motor neuron dispersion through the CN6 motor nuclei. Additionally, CN6 nerves failed to reach their target lateral rectus muscles (Figs. 6A–D). There was a statistically significant association between treatment group and the proportions of fish with CN6 phenotypes, but no statistically significant difference in survival (Figs. 6D, 6E). F2 germline *frmd4bb*$^{-/-}$ mutants (c.1687_1697delGATGAAATGAA, p.(Asp563ProfsTer25)) had phenotypes consistent with their G0 counterparts, including malformation of CN6 motor neuron nuclei and failed CN6 nerve extension toward target extraocular muscles relative to *frmd4bb*$^{+/+}$ fish (Figs. 6F, 6G). These phenotypes were also visible but poorly resolved by stereomicroscope and required manual adjustment of the focus through z-planes; thus phenotypes were poorly captured by stereomicroscope imaging of a single z-plane (Supplementary Fig. S3B).

Functional Testing of Transcription Factor Candidate Variants by Protein Binding Microarray

Our sequenced human oCCDD cohort included four pedigrees, each of which harbored a variant of uncertain significance in the DNA binding domain of one of four transcription factors. Pedigree 160 harbored c.411G>C (p.(Trp137Cys), ENST00000298231.5) in *PHOX2A*, a known CFEOM gene; Pedigree 232 harbored c.667G>A (p.(Glu223Lys), ENST00000373313.3) in *MAFB*, a known DRS gene; Pedigree ENG_ET harbored c.467G>T (p.(Arg156Leu), ENST00000333337.3) in *OLIG2,* a novel DRS candidate gene; and Pedigree 90 harbored c.742G>T, (p.(Ala248Ser), ENST00000342310.7) in *LMX1A*, a novel DRS candidate gene. Interestingly, *PHOX2A, MAFB,* and *OLIG2* but not *LMX1A* yielded the correct cranial motor nucleus/nerve phenotype after LOF CRISPR targeting in zebrafish. To couple the gene-level testing of our zebrafish screen with functional testing of these variants of uncertain significance, we mapped the variants relative to other reported variants in these proteins (Figs. 7A–C) and assessed transcription factor-DNA interactions by protein binding microarray (Figs. 7D–L).

For each variant, we performed universal protein binding microarray experiments[4,26] for a pair of reference (REF) and mutant (MUT) DNA binding domains on the same array and generated transcription factor binding site motif logos (Figs. 7D–F). For a quantitative view of each experiment, we analyzed the distribution of E-scores (rank-based enrichment score per DNA 8-mer ranging from -0.5 to 0.5, in which 0.5 indicates highly specific binding to that 8-mer, Figs. 7G–L).

PHOX2A p.(Trp137Cys) led to complete loss of binding to the wild-type PHOX2A motif, indicated by the degenerate motif logo for the mutant (Fig. 7D), and to a significant drop in E-scores for 8-mers resembling the wild-type motif to a level indistinguishable from that of the negative control (Figs. 7G, 7J).

Interestingly, MAFB p.(Glu223Lys) did not completely prevent transcription factor recognition of the wild-type motif (Fig. 7E). Nevertheless, the E-scores for the 8-mers recognized by the wild-type MAFB showed significantly lower values for the mutant DNA binding domain (Figs. 7H, 7K). The E-score distribution for the mutant was still higher than that of the negative control (Fig. 7K), which is indicative of partial loss of binding. This is consistent with the observation that the variant still permits the DNA binding domain to recognize the wild-type motif (Fig. 7E).

OLIG2 p.(Arg156Leu) led to a complete loss of binding to the wild-type OLIG2 motif, characterized by the degenerate mutant motif (Fig. 7F), and significant reduction in mutant E-scores for 8-mers recognized by wild-type OLIG2 to a level similar to that of the negative control (Figs. 7I, 7L). These data support that the tested missense variants may have a deleterious effect on protein function, but more data will be needed over time, including testing additional pathogenic and benign variants once their clinical impact has been established.

Finally, the motif generated from LMX1A (p.(Ala248Ser) was identical to the wild-type LMX1A motif, suggesting that this variant does not lead to complete loss of motif binding. However, the variant did lead to a very mild reduction in

Table. Human Probands' Clinical Phenotypes and Variants in Known and Novel oCCDD Candidate Genes Derived From the Zebrafish Screen

Pedigree ID	**160**	**232**	**ENG_CMK**	**ENG_ET**	**ENG_OA**
Diagnosis	Syndromic sporadic CFEOM	Isolated familial DRS	Syndromic sporadic CFEOM	Isolated familial DRS	Syndromic sporadic DRS
Sex assigned at birth	Male	Male	Male	Female	Female
Reported previously?	PMID: 39033378	PMID: 39033378	PMID: 39033378	PMID: 39033378	PMID: 39033378
Variants					
Variant (GRCh38/hg38)	chr11:72240193C>G	chr20:40688184C>T	chr3:50186688 C>A	chr21:33027329G>T	chr3:69302379 T>C
Gene	*PHOX2A*	*MAFB*	*SEMA3F*	*OLIG2*	*FRMD4B*
Variant (cDNA, protein)	c.411G>C, p.(Trp137Cys)	c.667G>A, p.(Glu223Lys)	c.1889C>A, p.(Ser630Ter)	c.467G>T, p.(Arg156Leu)	c.380A>G, p.(Lys127Arg)
Transcript	ENST00000298231.5	ENST00000373313.3	ENST00000002829.8	ENST00000333337.3	ENST00000398540.8
Inheritance	AR-hom	AD-inc	AR-hom	AD-inc	AR-hom
Ophthalmological					
CFEOM (HP:0001491)	Y, BL	N	Y, R side	N	N
Congenital ptosis (HP:0007970)	Y, severe BL, L>R side	N	Y, R side	N	N
Impaired ocular abduction (HP:0000634)	Y, abs BL	Y, abs BL	N	Y, BL	Y, L side
Impaired ocular adduction (HP:0000542)	Y, abs BL	Y, abs BL	N	Y, mild BL	Y, L side
Limited vertical eye movements	Y, severe BL	N	Y, unable to elevate or fully depress R eye	N	N
Duane anomaly (HP:0009921)	N	Y, type III BL	N	Y, type I BL, upshoot L side	Y, type III with upshoot L side
Hypotropia (HP:0025584)	Y, R side	N	N	Y	N
Exotropia (HP:0000577)	Y, L side	Y	Y, intermittent R side	N	Y, in R gaze
Esotropia (HP:0000565)	N	N	N	Y, alternating	N
Ophthalmologic surgeries	N	Y, LR muscle recessions of 8 mm R side and 6 mm L side	N	Y, initial 5.5 mm MR muscle recessions BL, secondary 1.0 MR muscle recessions BL	N
Other CN findings					
Absent Bell's phenomenon	Y, BL	N	N	N	N
CN8: Congenital sensorineural hearing impairment (HP:0008527)	N	N	Y, BL	N	? sensorineural vs conductive R side
Neurological					
Global developmental delay (HP:0001263)	N	N	Y	N	N
Delayed speech and language development (HP:0000750)	N	N	Y	N	Y
Delayed g ross motor development (HP:0002194)	N	N	Y	N	Y
Cognitive impairment (HP:0100543)	N	N	NA	N	N
Attention deficit hyperactivity disorder (HP:0007018)	N	N	N	N	Y
Panic attacks (HP:0025269)	N	N	N	Y	N
Infantile muscular hypotonia (HP:0008947)	N	N	Y	N	N
Unsteady gait (HP:0002317)	N	N	Y	N	N
Craniofacial					
Low-set, posteriorly rotated ears (HP:0000368)	N	N	Y	N	N
Protruding ears (HP:0000411)	N	N	Y	N	N
Upslanted palpebral fissures (HP:0000582)	N	N	Y	N	N
Wide nasal bridge (HP:0000431)	Y	N	N	N	N
Underdeveloped supraorbital ridge (HP:0009891)	Y	N	N	N	N

Table. Continued

Pedigree ID	160	232	ENG_CMK	ENG_ET	ENG_OA
Skeletal					
Overlapping toes (HP:0001845)	N	N	Y, 1st and 2nd toes BL	N	N
Short 2nd toe (HP:0001885)	N	N	Y, BL	N	N
Joint contracture of the 4th finger (HP:0009274)	N	N	Y, BL	N	N
Hypoplastic 5th fingernail (HP:0008398)	N	N	Y, BL	N	N
Short 5th finger (HP:0009237)	N	N	Y, BL	N	N
Volar fingernails (HP:0033976)	N	N	Y, 5th fingers and 2nd toes BL	N	N
Skeletal surgeries	N	N	Y, finger surgery	N	N
Cardiac					
Heart palpitations (HP:0001962)	NA	NA	N	NA	Y
Atrial septal defect (HP:0001631)	N	NA	N	NA	Y
Gastrointestinal					
Gastritis (HP:0005263)	N	N	N	N	Y
Gastroesophageal reflux (HP:0002020)	N	N	N	N	Y
Anorexia (HP:0002039)	N	N	N	N	Y
Decreased body weight (HP:0004325)	N	N	Y	N	N
Other findings					
Cafe-au-lait spots (HP:0000957)	N	N	Y	N	N
Snoring (HP:0025267)	N	N	Y	N	N
Bony protuberance in the ear	N	N	N	N	Y, R side
Brain MRI					
Abnl CN2 (HP:0000587)	Y, asymmetric positioning	NA	NA	NA	NA
Abnl CN3	Y, abs BL	NA	Y, hypo BL	NA	NA
Abnl CN7 (HP:0010827)	N	NA	N	NA	NA
Abnl CN8 (HP:0009591)	N	NA	Y, cochlear nerves abs BL, vestibular nerves hypo BL	NA	NA
Abnl extraocular muscles (HP:0008049)	Y, small MR, SO, and SR muscles BL	NA	Y, small MR and IR muscles BL, ? thin SR BL	NA	NA
Abnl medial temporal lobe	N	NA	Y, BL	NA	NA
Dysplastic corpus callosum (HP:0006989)	Y, drooping splenium	NA	Y, upward bowing	NA	NA
Hypo anterior commissure (HP:0030303)	N	NA	Y	NA	NA
Cochlear malformation (HP:0008554)	N	NA	Y, thickened modioli, abs cochlear apertures BL	NA	NA
Narrow IAC (HP:0011386)	N	NA	Y, BL with inferior outpouchings at the level of the fundi	NA	NA
Large nasopharyngeal adenoids (HP:0040261)	N	NA	Y	NA	NA
Abnl cerebral vascular morphology (HP:0100659)	Y, large vessel lateral to basilar artery	NA	N	NA	NA

Key: ?-possibly, abnl-abnormal, abs-absent, AD-inc-autosomal dominant with incomplete penetrance, AR-hom-autosomal recessive homozygous, BL-bilateral, CFEOM-congenital fibrosis of the extraocular muscles, CN-cranial nerve, CN2-optic nerve, CN3-oculomotor nerve, CN7-facial nerve, CN8-vestibulocochlear nerve, DRS-Duane retraction syndrome, hypo-hypoplastic, IAC-internal auditory canal, IR-inferior rectus muscles, L-left, LR-lateral rectus muscles, MR-medial rectus muscles, N-no, NA-not ascertainable/unknown, R-right, SO-superior oblique muscles, SR-superior rectus muscles, Y-yes.

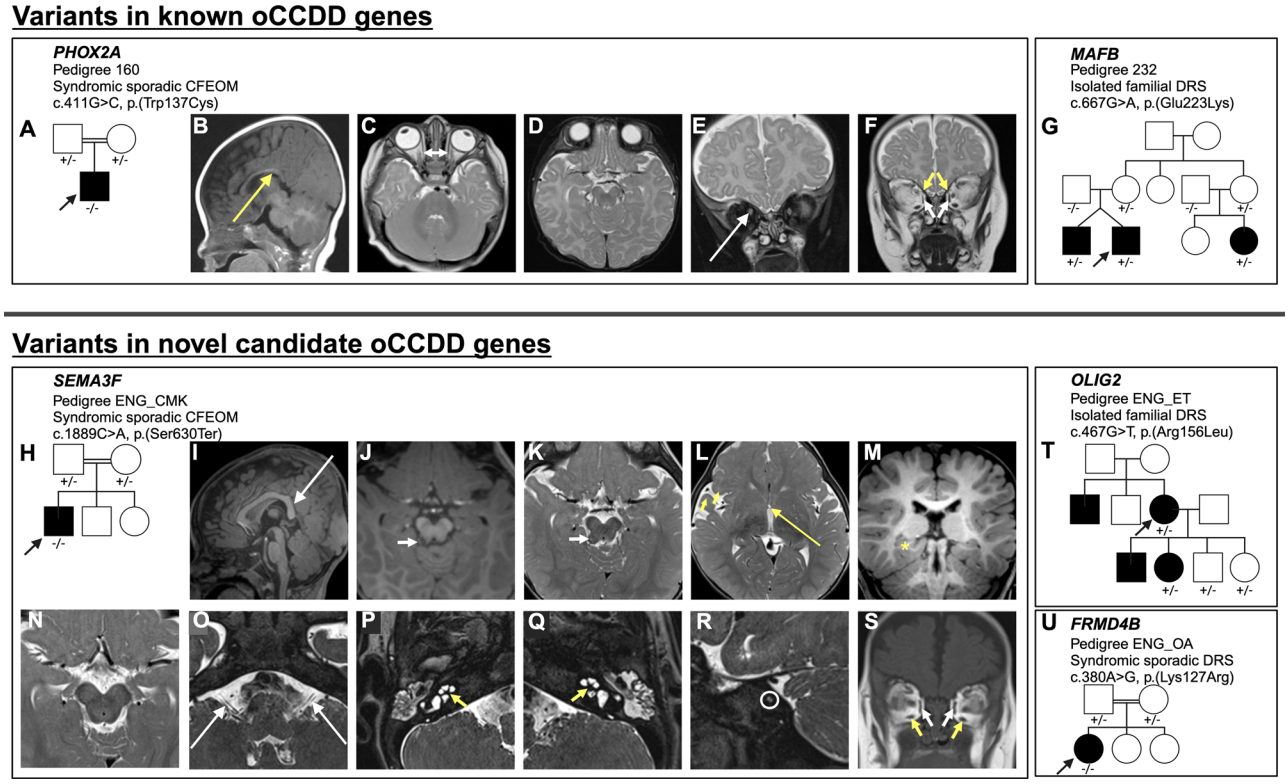

Figure 8. The oCCDD pedigrees with functionally validated candidate genes/variants and brain MR images of probands with homozygous *PHOX2A* and *SEMA3F* variants. (**A, G, H, T, U**) Schematics of pedigrees segregating variants of uncertain significance in known or novel candidate oCCDD genes. (**B–F**) Images from a 1.5T Siemens brain MRI of the pedigree 160 proband at four months of age that has CFEOM and harbors a homozygous *PHOX2A* variant. (**B**) Sagittal T1 fluid–attenuated inversion recovery 4 mm–thick image reveals abnormal anatomy of the corpus callosum with a somewhat down-slanted posterior body and splenium (*long yellow arrow*). (**C**) Axial turbo spin echo (TSE) T2-weighted 4 mm–thick image shows diminutive medial rectus muscles (*short double-headed white arrow*). (**D**) Axial TSE T2 weighted 4 mm thick image at the level of the midbrain and interpeduncular cistern does not show oculomotor nerves. (**E, F**) Coronal TSE T2-weighted 4 mm–thick images with and without fat-suppression show asymmetric positioning of the optic nerves, higher on the right (*long white arrow*), diminutive medial rectus muscles (*short white arrows*), and small superior oblique muscles (*short yellow arrows*). Because of slice thickness and slice angle, the superior rectus muscles were not as readily assessed but also appeared slightly small. (**I–S**) The ENG_CMK proband that has CFEOM and harbors a homozygous *SEMA3F* had MR imaging at 12 months of age obtained on a 3T Siemens Skyra (**I–M, O–S**) and three months of age obtained on a 1.5T Siemens unit (N) variant. I, Midline sagittal T1 magnetization prepared rapid gradient echo (MPRAGE) 1 mm–thick image demonstrates abnormal anatomy of the corpus callosum with a somewhat down-slanted posterior body and splenium (*long white arrow*). (**J**) Axial 1 mm reformatted MPRAGE and (**K**) 2.5 mm–thick TSE T2-weighted images show a small protuberance off or along the right side of the tectum (*short white arrows*) that appears hypointense on T1 and heterogeneous on T2 with central high-signal and peripheral low-signal intensity. This lesion is of uncertain etiology but was present in retrospect on an examination the previous year. (**L**) Axial 2.5–mm thick TSE T2-weighted image demonstrating a diminutive anterior commissure (*long yellow arrow*) and slight underdevelopment of the right frontal and temporal opercula (*short yellow arrow*). (**M**) Reformatted 1 mm coronal MPRAGE image shows asymmetry of the hippocampal formations and medial temporal lobes with the right side appearing mildly misshapen (*yellow asterisk*). N, Axial 2.5 mm–thick T2-weighted image at the level of the midbrain does not show oculomotor nerves at the level of the interpeduncular cistern; O, Axial 0.44 mm–thick T2 Sampling perfection with application optimized contrasts using different flip angle evolution (SPACE) image shows that the cisternal segments of the vestibulocochlear nerves are present but small (*long white arrows*) as they course posterior and parallel to the facial nerves. (**P, Q**) T2 SPACE images through the inner ears show dysmorphic, thickened cochlear modioli with stenotic cochlear apertures, more pronounced on the left (*short yellow arrows*). The apices of the cochleae appear mildly flattened. (**R**) Sagittal oblique T2 space MRI shows marked stenosis of the left internal auditory meatus (*white circle*) with only one cranial nerve visible instead of the expected four (facial, cochlear, and superior and inferior vestibular nerves). (**S**) Coronal 5 mm–thick T1-weighted image of the brain at the level of the orbits shows small medial rectus (*short white arrows*) and inferior rectus muscles (*short yellow arrows*). The superior rectus muscles are likely also small but are suboptimally assessed because of slice thickness.

binding to the wild-type motif, a finding of unclear significance (data not shown).

Additional Human Phenotyping of Pedigrees With Variants in PHOX2A, MAFB, SEMA3F, OLIG2, or FRMD4B

Additional cosegregation analysis and phenotyping are shown for the human pedigrees who harbored variants in *PHOX2A, MAFB, SEMA3F, OLIG2,* and *FRMD4B* (Table; Fig. 8, Supplementary Table S2). The variants in these genes were absent from the population and predicted to be damaging.

The proband of syndromic sporadic Pedigree 160 harbored the homozygous *PHOX2A* variant shown above to abrogate DNA binding (c.411G>C, p.(Trp137Cys); Table; Figs. 8A–F). He had bilateral CFEOM with severe, bilateral restrictions in vertical eye movements; absent horizontal eye movements; severe, bilateral congenital ptosis worse on the left side; exotropia; and right hypotropia. Brain

MRI revealed characteristic *PHOX2A*-associated anomalies, including indiscernible CN3 bilaterally and hypoplasia of the extraocular muscles typically innervated by CN3/CN4. Additional subtle syndromic features included mild craniofacial dysmorphisms and brain MRI findings consisting of asymmetric CN2 positioning, corpus callosal anomalies, and a prominent anomalous vessel that was likely venous in nature and coursed lateral to the basilar artery.

Three affected members of Pedigree 232 and their unaffected mothers harbored a partially penetrant heterozygous *MAFB* variant shown by protein binding microarray to reduce DNA binding (c.667G>A, p.(Glu223Lys); Table; Fig. 8G). The family segregated three subtypes of DRS in twins and a maternal first cousin. The proband had bilateral, exotropic DRS type III characterized by bilateral limitation of abduction and adduction and globe retraction on attempted adduction. He required two eye muscle surgeries to try to improve his eye alignment; both lateral rectus muscles were recessed in each procedure. His twin had bilateral, asymmetric esotropic DRS type I with limited abduction and globe retraction on adduction bilaterally, and their cousin had left-sided exotropic DRS type II with mildly restricted adduction and globe retraction on adduction, exotropia in upgaze, myopic astigmatism, and a right head turn.

The proband of syndromic sporadic consanguineous Pedigree ENG_CMK harbored a homozygous *SEMA3F* variant (c.1889C>A, p.(Ser630Ter), ENST00000002829.8) which localizes to the Ig-like domain involved in ligand binding and is predicted to result in nonsense-mediated mRNA decay (Table; Figs. 8H–S, Supplementary Fig. S4A, Supplementary Table S5).[27] He had syndromic right-sided CFEOM characterized by absent upgaze, limited downgaze, congenital ptosis, and intermittent exotropia. Syndromic features included bilateral sensorineural hearing impairment, mild facial dysmorphisms, and contractures and shortening of the fingers. Brain MRI revealed hypoplasia of CN3 bilaterally, hypoplasia of CN3-innervated extraocular muscles, small CN8, stenotic internal auditory meati, dysmorphic cochleae, corpus callosal anomalies, small anterior commissure, and asymmetric hippocampal formations and medial temporal lobes.

Two affected members of Pedigree ENG_ET harbored a partially penetrant heterozygous *OLIG2* variant shown above to abolish DNA binding (c.467G>T, p.(Arg156Leu); Table; Fig. 8T). The proband and her daughter had DRS, and the proband's unenrolled brother and son had DRS by report. The proband had bilateral esotropic type I DRS requiring two bilateral medial rectus muscle recessions and characterized by impaired abduction and mildly impaired adduction bilaterally, left-sided upshoot, and hypotropia. The daughter of the proband had right-sided esotropic DRS type I with restricted abduction and globe retraction on adduction. Of note, two unaffected children of the proband also harbored the variant.

Finally, syndromic sporadic DRS proband ENG_OA harbored a homozygous *FRMD4B* variant (c.380A>G, p.(Lys127Arg), ENST00000398540.8) located in the Band 4.1 domain, which is involved in cytoskeletal-membrane linkage (Fig. 8U, Supplementary Fig. S4B).[27] She had left-sided exotropic DRS type III characterized by impaired abduction and adduction, globe retraction in adduction, and upshoot. Syndromic features included hearing impairment, delayed speech and walking, atrial septal defect, and gastrointestinal abnormalities.

Discussion

Historically, linkage analysis and DNA sequencing of pedigrees segregating oCCDDs have led to the identification of recurrently mutated genes.[28–30] More recently, our exome/genome sequencing of 467 genetically unsolved oCCDD pedigrees yielded many candidate genes/variants of uncertain significance mutated in just one pedigree.[3] Here, our functional evaluation of a subset of these genes/variants of uncertain significance using a G0 LOF zebrafish screen and protein binding microarray further supports the oCCDD involvement of five of these.

In zebrafish, G0 and F2 LOF of known (*phox2a, mafba*) and novel (*sema3fa, olig2, frmd4bb*) oCCDD genes led to ocular cranial motor neuron developmental phenotypes. In addition, protein binding microarray testing of candidate variants in transcription factors supported the functional effects of human sequence-derived missense alleles in known and novel candidate oCCDD genes *PHOX2A, MAFB*, and *OLIG2*.

As in homozygous LOF germline models, G0 targeting of *phox2a* resulted in loss of CN3/CN4 motor nuclei in zebrafish. Moreover, the PHOX2A p.(Trp137Cys) substitution resulted in CFEOM in a human proband and complete loss of transcription factor-DNA binding in vitro. Although missense alleles that localize to the DNA binding domain and predicted LOF alleles have been reported as pathogenic for *PHOX2A*-CFEOM,[1,31] the functional effects of these alleles were not demonstrated. Thus this is the first reported *PHOX2A*-CFEOM candidate missense allele that localizes to the DNA binding domain and is demonstrated to abolish transcription factor-DNA binding.

G0 targeting of the known DRS gene *mafba* resulted in germline homozygous null-equivalent phenotypes. Moreover, MAFB p.(Glu223Lys) resulted in reduced transcription factor-DNA binding, and the variant cosegregated with incomplete penetrance in a DRS pedigree. Although reported human alleles have demonstrated reduced penetrance for DRS and other *MAFB*-associated phenotypes,[2,32–34] functional tests of human *MAFB*-DRS alleles have thus far demonstrated haploinsufficiency or dominant negative consequences. Two DRS alleles have been reported in the MAFB DNA binding domain,[2,32,35] but their effects on DNA binding have not been demonstrated.

SEMA3F encodes a semaphorin involved in axon guidance. Similar to proband ENG_CMK who had CFEOM, developmental delay, sensorineural hearing impairment, and an MRI revealing small CN3 (and inability to resolve CN4), absent CN8, and brain malformations, *Sema3f*$^{-/-}$ mice have CN3 defasciculation and CN4 absence consistent with CFEOM, as well as hearing impairment and brain malformations.[36,37] Although our zebrafish LOF models also had CN3 defasciculation, CN4 was grossly intact, suggesting that this phenotype may have species-specific differences (Supplementary Table S5). Interestingly, a single ClinVar submitter reported a human proband with hearing impairment and a *SEMA3F* missense variant of uncertain significance and unspecified zygosity localizing to the same Ig-like domain as the variant harbored by proband ENG_CMK (c.1849G>A, p.(Val617Met), Variation ID: 1064910; Supplementary Fig. S4A), supporting putative association between *SEMA3F* variants and hearing impairment.[38] Notably, human heterozygous *SEMA3F* missense variants of uncertain significance localizing to diverse SEMA3F protein domains were

Investigative Ophthalmology & Visual Science

previously described in individuals with hypogonadotropic hypogonadism with or without anosmia who were not reported to have CFEOM, hearing impairment, or other syndromic features in proband ENG_CMK (Supplementary Fig. S4A).[39] Three of these reported *SEMA3F* variants were tested functionally and led to impaired protein secretion *in vitro* (p.(Thr29Met), p.(Pro452Thr), and p.(Thr724Met)). Although one variant (p.(Ala652Ser)) localized to the SEMA3F Ig-like domain, its functionality was not tested. Moreover, the proband harboring this variant also harbored a variant in *FGFR1* (p.(Arg209Cys)) which is reported as likely pathogenic for hypogonadotropic hypogonadism with or without anosmia in ClinVar (Variation ID: 548670), suggesting that this is a possible alternative explanation for the phenotype in this proband. Neither the ENG_CMK proband nor his carrier parents were noted to have anosmia or hypogonadism, but these phenotypes may have been missed in the proband due to his developmental delays and evaluation before typical pubertal onset. Alternatively, this may be attributable to the distinct nature of the proband's homozygous nonsense variant, which is predicted to induce nonsense-mediated mRNA decay. Additional studies are required to reconcile the differences in functional consequences of variants among probands with *SEMA3F* variants.

Our G0 and F2 LOF studies and others' published morpholino knockdown studies[40] support that *olig2* LOF results in loss of CN6 nuclei in zebrafish, consistent with DRS. Moreover, OLIG2 is downstream of the known DRS protein MAFB,[15] and human GWAS has associated *OLIG2* SNPs with DRS.[41] By protein binding microarray, OLIG2 p.(Arg156Leu) resulted in a complete loss of transcription factor-DNA binding, consistent with the LOF mechanism tested by our zebrafish assay.

FRMD4B encodes a poorly characterized scaffolding protein involved in processes including cytoskeletal dynamics and protection against retinal dysplasia in mice.[42] Though LOF of zebrafish *frmd4bb* results in a CN6 phenotype, *FRMD4B* is mutated in only one DRS proband in our cohort, whose specific missense variant remains untested.

In summary, because this is the first report of a *PHOX2A*-CFEOM missense variant in the DNA binding domain, pathogenicity of the p.(Trp137Cys) PHOX2A allele remains incompletely proven but is strongly suspected. Moreover, although two *MAFB*-DRS missense variants in the DNA binding domain have been reported, reduced DNA binding has not yet been demonstrated as a pathogenic mechanism. Finally, because *SEMA3F*, *OLIG2*, and *FRMD4B* are each mutated in a single pedigree in our cohort, additional human alleles resulting in a similar phenotype are needed to prove pathogenicity. However, these are now strong oCCDD candidate genes.

Identifying the primary downstream regulatory targets of transcription factors PHOX2A, MAFB, and OLIG2 is of great interest, as this could elucidate novel insights into the neurodevelopmental pathways required for cranial motor neuron development. Although bioinformatic tools can predict regulatory targets from publicly available functional datasets, their outputs are of uncertain relevance to oCCDDs, because transcription factor regulatory networks are often highly specific to cell type and developmental time point. However, some published literature provides insights into these networks. The *OLIG2*, *PHOX2A*, and *MAFB* genes encode pleiotropic transcription factors that bind to specific short noncoding DNA consensus motifs to activate or repress the expression of target genes in a cell-type specific fashion, and all are critical to the development of specific pools of cranial motor neurons. The developing embryonic hindbrain is transiently segmented into eight rhombomeres defined by the combined expression of *HOX* genes and additional transcription factors. The abducens nucleus forms in rhombomeres 5 and 6. The formation of these two rhombomeres is dependent on the regional expression of *Mafb* and the binding of MAFB to its consensus motif, the Maf recognition element, to direct the downstream expression of *Hoxa3* and *Hoxb3*.[17,43–47] In the absence of *Mafb,* these rhombomeres, and thus the abducens nucleus, fails to develop.[15–17] After the establishment of rhombomeres 5 and 6, the differentiation of abducens motor neuron progenitors is dependent on the expression of the transcriptional repressor, *Olig2,* which specifies both subtype identity and pan-neuronal properties of developing motor neurons by controlling the expression of downstream genes such as *Isl1* and *Hb9*.[48] In the absence of *Olig2,* these progenitors remain in the cell cycle and fail to produce abducens motor neurons.[40] *Phox2a* and its paralog, *Phox2b,* are key to the generation and survival of a subset of brainstem motor neurons and adrenergic neurons. Their onset of expression is asynchronous, and in oculomotor and trochlear progenitors, *Phox2a* is upstream of *Phox2b.* In chick, *Phox2a* specifies oculomotor and trochlear cell fate and orchestrates the formation of the corresponding motor nuclei.[49] Loss of *Phox2a* in mice,[12] zebrafish,[24] and humans[13] leads to the absence of oculomotor and trochlear nuclei. Mouse embryonic stem cells can be differentiated to oculomotor-like motor neurons through the expression of *Ngn2, Isl1*, and *Phox2a*. Chromatin immunoprecipitation-sequencing analysis revealed that the oculomotor-like cell fate was programmed by the synergistic interaction of Isl1 and Phox2a, with the recruitment of Isl1-Phox2a complexes to distinct genomic locations in a cell type-specific fashion.[50] Together, these foundational studies and the functional evidence that we present here suggest the value of additional elucidation of these regulatory network targets through newer methods such as CUT&Tag and RNA-seq.

The G0 screening method we use in the present study has limitations. First, because phenotypes were screened at 72 hpf under the stereomicroscope, later-onset or less-robust phenotypes may have been missed. Because many positive hits from our screen were transcription factors with obvious LOF phenotypes, focusing future screens on conserved transcription factors with known cranial motor neuron expression may lead to improved success rates. Second, our screen may not have captured LOF of all genes tested, because phenotype induction depends on interspecies conservation, mutant viability, and guide RNA and injection efficiencies (guide RNAs were not prevalidated), and because knockout of both paralogs of duplicated genes may be needed for phenotypic manifestation. Moreover, because LOF was not confirmed at the mRNA or protein levels, some may have resulted in partial LOF, resulting in incomplete phenotype manifestation. Third, the screen only examines the outcome of biallelic LOF of the tested gene; by contrast, many of the human variants were monoallelic or missense and may act through alternative non-LOF mechanisms. Finally, because zebrafish lack eyelids and the levator palpebrae superioris muscle that elevates them, we were able to assess three ptosis and four MGJWS candidate genes for gross CN3 or CN5 abnormalities but not for ptosis-specific CN3 vulnerabilities. Moreover, testing of DRS candidate genes in the HGj4A line enabled assessment of primary CN6 abnormalities, but

Investigative Ophthalmology & Visual Science

not of the additional CN3 misinnervation characteristic of human DRS. For these collective reasons, we cannot definitively exclude candidates that screened negative.

Despite these limitations, our study has identified three strong novel oCCDD candidate genes and has demonstrated functionality of candidate variants in transcription factors. Our findings support that human sequence analysis can be coupled with G0 LOF screening in zebrafish and targeted functional assays to aid in the prioritization of candidate genes (Supplementary Files).

Acknowledgments

The authors thank David Schoppik and Paige Leary for sharing their invaluable expertise in zebrafish imaging.

Supported in part by NEI R01EY027421 and NHLBI X01HL132377 (E.C.E). Human sequencing and analysis were provided by the Broad Institute Center for Mendelian Genomics (Broad CMG) and were funded in part by the NHGRI grant UM1HG008900, with additional support from NEI and NHLBI; these data are available through dbGaP project number phs001272.v2.p1. Additionally, the human sequencing results analyzed and published here are based in part upon data generated by Gabriella Miller Kids First Pediatric Research Program project phs001247.v1.p1 and were accessed from the Kids First Data Resource Portal (https://kidsfirstdrc.org/) and/or dbGaP (www.ncbi.nlm.nih.gov/gap). Analysis was also supported by NHGRI grants U01HG011755 and R01HG009141, NIMH grant MH115957, along with grant 2022-309464 from the Chan Zuckerberg Initiative DAF, an advised fund of Silicon Valley Community Foundation. J.A.J. was supported by T32GM007748, T32NS007473, T32EY007145, and the Harvard Medical School William Randolph Hearst Fund. P.M.M.R. was supported by R01 EY027421-02S1 and R01 EY027421-04S1. M.C.W. was supported by NEI 5K08EY027850, NEI R01EY032539, and the BCH Ophthalmology Foundation Faculty Discovery Award. D.G.M. acknowledges a National Health and Medical Research Council investigator grant (#2009982). M.C.W., S.M., and D.G.H. receive research support from Children's Hospital Ophthalmology Foundation, Inc., Boston, MA. K.A. and K.K. were supported by an NBRP grant from AMED. We acknowledge KAKENHI grant number JP25830020 (K.A.) and an NBRP grant from MEXT (K.K.). This work was conducted with support from Harvard Catalyst | The Harvard Clinical and Translational Science Center (National Center for Advancing Translational Sciences, NIH UL1TR002541 and financial contributions from Harvard University and its affiliated academic healthcare centers. The content is solely the responsibility of the authors and does not necessarily represent the official views of Harvard Catalyst, Harvard University and its affiliated academic healthcare centers, or the National Institutes of Health. This study was supported in part by NHGRI R01HG010501 (M.L.B.) and by NICHD R03HD099358 (M.L.B.). E.C.E. is a Howard Hughes Medical Institute Investigator.

Disclosure: **J.A. Jurgens**, None; **P.M. Matos Ruiz**, None; **J. King**, None; **Emma E. Foster**, None; **L. Berube**, None; **W.-M. Chan**, None; **B.J. Barry**, None; **R. Jeong**, None; **E. Rothman**, None; **M.C. Whitman**, None; **S. MacKinnon**, None; **C. Rivera-Quiles**, None; **B.M. Pratt**, None; **T. Easterbrook**, None; **F.M. Mensching**, None; **S.A. Di Gioia**, Regeneron Pharmaceutical (E); **L. Pais**, None; **E.M. England**, None; **T. de Berardinis**, None; **A. Magli**, None; **F. Koc**, None; **K. Asakawa**, None; **K. Kawakami**, None; **A. O'Donnell-Luria**, Pacific Biosciences (F), Addition Therapeutics (C, F), Tome Biosciences (C, F), Ono Pharma USA (C, F); **D.G. Hunter**, Rebion (O, P); **C.D. Robson**, None; **M.L. Bulyk**, U.S. patents #6,548,021 and #8,530,638 on PBM technology and corresponding universal sequence designs (P); **E.C. Engle**, None

References

1. Bosley TM, Oystreck DT, Robertson RL, al Awad A, Abu-Amero K, Engle EC. Neurological features of congenital fibrosis of the extraocular muscles type 2 with mutations in PHOX2A. *Brain*. 2006;129(Pt 9):2363–2374.
2. Park JG, Tischfield MA, Nugent AA, et al. Loss of MAFB function in humans and mice causes duane syndrome, aberrant extraocular muscle innervation, and inner-ear defects. *Am J Hum Genet*. 2016;98:1220–1227.
3. Jurgens JA, Barry BJ, Chan WM, et al. Expanding the genetics and phenotypes of ocular congenital cranial dysinnervation disorders. *Genet Med*. 2024;27(4):101216.
4. Berger MF, Bulyk ML. Universal protein-binding microarrays for the comprehensive characterization of the DNA-binding specificities of transcription factors. *Nat Protoc*. 2009;4:393–411.
5. Kock KH, Kimes PK, Gisselbrecht SS, et al. DNA binding analysis of rare variants in homeodomains reveals homeodomain specificity-determining residues. *Nat Commun*. 2024;15(1):3110.
6. Fadool JM, Dowling JE. Zebrafish: a model system for the study of eye genetics. *Prog Retin Eye Res*. 2008;27:89–110.
7. Amberger JS, Bocchini CA, Scott AF, Hamosh A. OMIM.org: leveraging knowledge across phenotype-gene relationships. *Nucleic Acids Res*. 2019;47(D1):D1038–D1043.
8. Howe K, Clark MD, Torroja CF, et al. The zebrafish reference genome sequence and its relationship to the human genome. *Nature*. 2013;496(7446):498–503.
9. Clark C, Austen O, Poparic I, Guthrie S. α2-Chimaerin regulates a key axon guidance transition during development of the oculomotor projection. *J Neurosci*. 2013;33:16540–16551.
10. Higashijima S, Hotta Y, Okamoto H. Visualization of cranial motor neurons in live transgenic zebrafish expressing green fluorescent protein under the control of the islet-1 promoter/enhancer. *J Neurosci*. 2000;20:206–218.
11. Asakawa K, Higashijima SI, Kawakami K. An mnr2b/hlxb9lb enhancer trap line that labels spinal and abducens motor neurons in zebrafish. *Dev Dyn*. 2012;241:327–332.
12. Pattyn A, Morin X, Cremer H, Goridis C, Brunet JF. Expression and interactions of the two closely related homeobox genes Phox2a and Phox2b during neurogenesis. *Development*. 1997;124:4065–4075.
13. Nakano M, Yamada K, Fain J, et al. Homozygous mutations in ARIX(PHOX2A) result in congenital fibrosis of the extraocular muscles type 2. *Nat Genet*. 2001;29:315–320.
14. Goldblatt D, Rosti B, Hamling KR, et al. Motor neurons are dispensable for the assembly of a sensorimotor circuit for gaze stabilization. *Elife*. 2024;13:RP96893.
15. Asakawa K, Kawakami K. Protocadherin-mediated cell repulsion controls the central topography and efferent projections of the abducens nucleus. *Cell Rep*. 2018;24:1562–1572.
16. Ma LH, Grove CL, Baker R. Development of oculomotor circuitry independent of hox3 genes. *Nat Commun*. 2014;5:4221.
17. Moens CB, Cordes SP, Giorgianni MW, Barsh GS, Kimmel CB. Equivalence in the genetic control of hindbrain segmentation in fish and mouse. *Development*. 1998;125:381–391.
18. Shah AN, Davey CF, Whitebirch AC, Miller AC, Moens CB. Rapid reverse genetic screening using CRISPR in zebrafish. *Nat Methods*. 2015;12:535–540.
19. Shankaran SS, Dahlem TJ, Bisgrove BW, Yost HJ, Tristani-Firouzi M. CRISPR/Cas9-directed gene editing for the generation of loss-of-function mutants in high-throughput zebrafish F screens. *Curr Protoc Mol Biol*. 2017;119:31.9.1–31.9.22.

Index of Supplementary Methods, Results, and Figures

Five additional supplementary tables accompany the manuscript. These have been uploaded as a separate supplementary spreadsheet:

Supplementary Table 1. Human sequence-derived candidate genes and variants and their conservation in fish.

Supplementary Table 2. Miscellaneous phenotypic and genetic details of human pedigrees.

Supplementary Table 3. Gene-targeting and scrambled guide RNAs, sequencing primers, and genomic sequences targeted with zebrafish CRISPR screen.

Supplementary Table 4. G0 mosaic versus F2 germline mutant phenotypes for novel oCCDD candidate genes in zebrafish at 72 hpf.

Supplementary Table 5. Comparison of phenotypes in human, zebrafish, and mouse models of SEMA3F missense or loss of function variants.

SUPPLEMENTARY METHODS

Prioritization of human sequence-derived alleles for screening in zebrafish

In our previous study, we leveraged human genetics to prioritize novel oCCDD candidate genes/ variants through phenotyping and exome/ genome sequencing of a large cohort of human pedigrees with oCCDDs.[1] Candidate genes/ variants were prioritized through multiple modalities including allele frequency filtering, predictive scores, pedigree-based analyses, identification of recurrently mutated genes and recurrent variants, annotation of animal models in the Monarch database, *de novo* variant analyses, and gene ontology analyses. In the present study, we further prioritized these candidate genes and variants based on amino acid-level conservation between human and zebrafish, recessive inheritance, and/or putative loss-of-function (LOF) consequences of the candidate variants (defined as stopgain, stoploss, frameshift, or splice site variants). Several human pedigrees had additional novel candidate genes/ variants which were not highlighted in our previous study, but which were also prioritized for the zebrafish screen based on conservation in fish, published literature, *in silico* predictors, and/or putative LOF consequences of the variant.

Sanger validation and cosegregation analysis of human sequence-derived variants

Sanger sequence validation was performed for candidate variants in genes that 1) yielded cranial motor phenotypes in both G0 and F2 mutants in our zebrafish screen, and/or 2) encoded transcription factors that were prioritized for protein binding microarray testing. PCR primers were designed using Primer3 v4.1.0[2] and assessed for specificity of amplification relative to other sites in the human genome (build GRCh38) using BLAT.[3] Sanger sequencing was performed for validation of variants in the probands and cosegregation analysis in additional pedigree members, when available (Supplementary Table 2).

Classification and computational prediction of human sequence-derived variants

Human variants were classified using criteria from the American College of Genetics and Genomics and Association for Molecular Pathology (ACMG/AMP),[4] with additional classification specifications from the Clinical Genome Resource (ClinGen) Variant Curation Committee (ClinGen General Sequence Variant Curation Process v1.0; https://www.clinicalgenome.org/site/assets/files/3677/clingen_variant-curation_sopv1.pdf; Supplementary Table 1). Computational predictions of missense variant deleteriousness were derived using REVEL.[5]

Guide RNA design and synthesis

Using CHOPCHOP[6–8] (accessed November 2018 (v2) and February 2020 (v3)), the eight highest-ranked guide RNAs (gRNAs) per target gene without predicted protein-coding off-target sites were selected. gRNAs that were also represented in a published 4-guide lookup table were prioritized.[9] When possible, gRNAs targeting coding sequences at least 50 bp upstream of the penultimate exon-exon junction were selected to induce nonsense-mediated mRNA decay.[10] The top four remaining guides with the fewest predicted off-target effects and highest predicted efficiencies were selected, and PAM sequences were omitted. Each of the four guides was submitted to the Genscript scrambled sequence generator to identify non-targeting scrambled guide control sequences. The first 2 nucleotides of gene-targeting and scrambled guides were modified to start with “GG” and flanked with a 5’ and 3’ sequence (TAATACGACTCACTATA; GTTTTAGAGCTAGAAATAGC) to generate top-strand oligos for annealing (Supplementary Table 3). The four top-strand gene-targeting or scrambled control oligos per gene were pooled (final pooled concentration 0.2 uM) and annealed with a universal bottom-strand ultramer (Integrated DNA Technologies, final concentration 0.2 uM) as

described.[11] *In vitro* transcription was performed using the MEGAscript T7 Transcription Kit (Thermo Fisher Scientific, Cat #AM1334) following the manufacturer's protocol, except for overnight incubation (≤16 hours) to increase RNA yield. RNA was purified using RNA Clean and Concentrator-5 kit (Zymo, Cat #R1016) following the manufacturer's protocol, except for use of an 8 uL elution volume to concentrate RNA.

Guide RNA/Cas9 complex formation and microinjection

Alt-R S.p. Cas9 Nuclease V3 (Integrated DNA Technologies, Cat #1081059) was diluted to yield a 10 uM Cas9 solution in 20 mM Tris-HCl, 600 mM KCl, and 20% glycerol and stored at -20°C. Cas9 solution and gRNAs were mixed for a final concentration of 5 uM Cas9, 1 ug/uL gRNA. When guides were pooled, four gRNAs were mixed such that total gRNA concentration remained 1 ug/uL. Cas9/gRNA mixture was incubated at 37° C for 5 minutes to generate Cas9/RNP complexes. The yolks of single-cell stage embryos were microinjected with 0.5-1.0 nL of Cas9/gRNA mixture.

Zebrafish husbandry

Zebrafish experiments were approved by the BCH Institutional Animal Care and Use Committee, and standard fish care was performed by the BCH Aquatic Resources Facility. Zebrafish were maintained on a standard 14 hour light/10 hour dark cycle at 28.5^{o}C. Before being added to the system at 5 dpf, embryos and larvae were maintained in 10 cm dishes with 30 mL of sterile fish water and densities of 30-50 fish per dish. For embryos younger than 24 hpf, water was supplemented with 0.5 ppm methylene blue. To avoid long-term isolation, individually genotyped adult fish were tagged with identifiable visible implant elastomers and

housed in groups (Northwest Marine Technology, 2017).[12]

G0 screening and F2 germline validation in LOF zebrafish models of prioritized genes

Experiments targeting CFEOM, ptosis, and MGJWS or DRS candidate genes were conducted in *Tg(isl1:GFP)*[13] or HGj4A *mnr2b/hlxb9lb*[14] reporter fish, respectively. The *Tg(isl1:GFP)* reporter line was originally generated through transgenic introduction of a linearized GFP-tagged *islet1* promoter/enhancer sequence, and the HGj4A line was made by *Tol2* transposition-mediated enhancer trapping to introduce a GFP construct upstream of the *mnr2b/hlxb9lb* gene.

Zebrafish embryos were generated using timed incrosses of adult reporter fish. G0 targeting experiments consisted of microinjecting single cell-stage embryos with four high dose (1ug/uL) guide RNAs redundantly targeting each gene.[9] Following injections, dead embryos and debris were removed twice daily. Live embryos were incubated at 28.5°C and counted every 24 hours until 72 hours post-fertilization (hpf). Sterile fish water with 0.2 mM N-Phenylthiourea, ≥98% (Sigma-Aldrich, Cat #P7629-100G) was added at 24 hpf to inhibit pigmentation/ melanization and replaced every 24 hours.

At 72 hpf, injected G0 fish were assessed using the Nikon SMZ1500 fluorescent stereomicroscope and NIS Elements AR 5.21.03 software to assess for gross phenotypic changes in cranial motor neuron nuclei and/or nerves. To visualize abnormalities at multiple z plane levels within each fish, we manually adjusted the focus level of the stereomicroscope through multiple z planes that collectively encapsulated the anatomic regions of interest. Fish were assessed for absent or malformed motor nuclei and aberrant axonal projections of CN3, CN4, and CN5 (*Tg(isl1:GFP)* fish) or CN6 (HGj4A fish). Preliminary G0 fish phenotypes were

derived from single experimental replicates without detailed phenotyping. Two additional G0 experimental replicates and F2 germline mutant validations were performed for genes whose targeting induced putative cranial motor nucleus/ nerve phenotypes in at least a subset of injected fish; these additional experiments were performed with confocal imaging.

Zebrafish confocal image acquisition and processing

G0 fish with putative cranial nucleus/ nerve phenotypes visualized under the stereomicroscope and F2 germline fish were additionally phenotyped using confocal imaging. G0 mutants were phenotyped blindly relative to wild-type uninjected or scrambled guide RNA-injected clutchmates. Imaging was performed on fish from at least three independent clutches for both G0 and F2 experiments. At 72 hpf, zebrafish were anesthetized and mounted dorsally in 1% low melting point agarose (ThermoFisher Scientific, Cat #16520100) in fish water in FluoroDishes (World Precision Instruments, Cat #FD3510). Fish were live imaged with a Zeiss LSM980 series upright laser scanning confocal microscope with a 20X water dipping objective (Cat #421452-9800-000). Images were acquired using Zen Software (Carl Zeiss MicroImaging GmbH, Göttingen, Germany) with 1024x1024 pixels, scan speed of 5, and 1 µM z-stacks.

Three-dimensional confocal z-stack images were processed using Arivis Vision4D software v4.0. The purpose of image processing was to improve standardization of experimentally-matched images and, when necessary, to remove non-cranial motor neuron/nerve anatomic structures that would otherwise obscure the pertinent anatomic features highlighted within each mutant. Image processing consisted of: 1) rotating images so that key anatomic structures were captured in a standard manner within a single 2-dimensional X-Y plane of control and mutant fish imaged in the same experiment; 2) transforming pixels back to their original dimensions for each image; 3) cropping and setting equivalent zoom levels for experimentally-matched images so that the same anatomic structures were encompassed within each; 4) creating a standard-sized scale bar in the 2D z-plane in which a standard

anatomic landmark was present for all experimentally-matched images; 5) digitally masking extreme autofluorescence from the zebrafish eyes and skin, which would otherwise obscure the cranial motor neuron/ nerve anatomy of interest; 6) for sema3fa images, manual cropping of non-CN3 anatomic structures to show only the pertinent anatomy in processed images; 7) generating a high-resolution 3D rendering of the final image. Raw unprocessed confocal images are provided for G0 and F2 fish (Supplementary Figures 1 and 2).

Protein structural mapping and universal protein binding microarray testing of transcription factor candidate variants

For genes/variants that were positively validated through the zebrafish screen and/or protein binding microarrays, 2D protein structural maps were generated based on domain annotations in InterPro v101.0.[15] Variants identified in our cohort were mapped relative to variants previously reported in the literature or in ClinVar[16] for isolated or syndromic oCCDD-related phenotypes.

As described previously,[17] protein binding microarrays were used to assess DNA binding capabilities of variants of uncertain significance in the DNA binding domains of known (*PHOX2A, MAFB*) or novel (*OLIG2, LMX1A*) transcription factor-encoding candidate genes relative to their wild-type counterparts. Human candidate variants were nominated for testing by protein binding microarray based on the following criteria: 1) the gene was tested in the zebrafish assay, 2) the variants localized to the DNA binding domain of a transcription factor, 3) the transcription factor class is known to express well in protein purification experiments, 4) and if the transcription factor-encoding gene had prior oCCDD association, the oCCDD phenotype in the human pedigree in the current cohort was consistent with that previously ascribed to the gene. On this basis, we selected the following four variants for testing by protein binding microarray: c.411G>C (p.(Trp137Cys), ENST00000298231.5) in *PHOX2A*, a known CFEOM gene; c.667G>A (p.(Glu223Lys), ENST00000373313.3) in *MAFB*, a known DRS gene;

c.467G>T (p.(Arg156Leu), ENST00000333337.3) in *OLIG2*, a novel DRS candidate gene; and c.742G>T, (p.(Ala248Ser), ENST00000342310.7) in *LMX1A*, a novel DRS candidate gene.

For protein binding microarray experiments, gBlock Gene Fragments encoding the DNA binding domains of human PHOX2A, MAFB, and OLIG2 were synthesized as double-stranded DNA fragments purchased from Integrated DNA Technologies. These fragments were cloned into a Gateway cloning-compatible entry vector, pDONR-221 (Invitrogen, Cat#12536017). Mutations PHOX2A-p.(Trp137Cys), MAFB-p.(Glu223Lys), OLIG2-p.(Arg156Leu), and LMX1A-p.(Ala248Ser) identified from human oCCDD exome or genome sequences were introduced into the vectors using QuickChange site-directed mutagenesis (Agilent, Cat#200519) and mutagenic PCR primers optimized according to the QuickChange primer design manual. Sequence verification was performed using Sanger sequencing through the Harvard Medical School Biopolymers Facility to confirm correct mutagenesis. Subsequently, wild-type and mutant constructs were cloned into N-terminal GST-tagged Gateway-compatible pDEST15 vectors (Invitrogen, Cat#11802014) and confirmed again by Sanger sequencing.

Wild-type and oCCDD mutant transcription factor DNA binding domain proteins were expressed using PURExpress in vitro transcription/translation Protein Synthesizer Kits (NEB, Cat#E6800L) in the same batch. Protein expression and correct size were validated by Western blot using rabbit anti-GST primary antibody (Sigma, Cat#G7781) and goat anti-rabbit secondary antibody (Pierce, Cat#31460). Protein concentration was quantified from the Western blots using GST protein standards (Pierce, Cat#20237) and analyzed with ImageJ software.[18]

Protein binding microarrays were prepared by following a standard double-stranding primer extension reaction with ThermoSequenase DNA Polymerase (Cytiva, Cat#E790000Y), unlabeled dNTPs (NEB, Cat#N0447S**)**, and fluorescently labeled Cy3-dUTPs (Cytiva, Cat#PA53022**)**. Arrays were then scanned for Cy3 signal at 523 nm with a 500 lp filter and analyzed using the Double Stranding Analysis pipeline. Wild-type and oCCDD mutant DNA binding domains were assessed using a custom-designed Universal Protein Binding Microarray

(8 x 60K GSE format, AMADID #030236; Agilent Technologies, Inc.) in phosphate-buffered saline (PBS) buffer.

Wild-type and mutant PHOX2A proteins were assayed at a concentration of 400nM on the PBM. Wild-type and mutant MAFB and OLIG2 proteins were assayed at a concentration of 600nM on the PBM. Each wild-type DNA binding domain and its corresponding mutant were tested in a separate chamber on the same array. Following protein binding, arrays were incubated with Alexa Fluor 488-conjugated anti-GST antibody (Invitrogen, Cat#A-11131) for fluorescent detection. Protein binding microarrays were then scanned using a GenePix 4400A microarray scanner. GPR files were generated using GenePix Pro 7.0 software at settings of 500, 400, and 300 PTM. Analysis of GPR files was performed using the Bulyk Lab PBM Universal Analysis Suite.

Motif logos were generated from protein binding microarray results using the Seed-and-Wobble method, as described previously.[19,20] Briefly, the top-scoring protein binding microarray 8-mer was used to generate a seed sequence. For each nucleotide within the seed, an E-score was derived from testing the relative preference of each possible nucleotide substitution at that site. For each nucleotide, scores were then converted to substitution probabilities using the Boltzmann distribution and shown as motif logos.

Figure generation

Figure schematics were created with BioRender.com using an academic license through Boston Children's Hospital. Licenses for main figures: WL27S2W9EK, KL27S1KJPP, YS27S1KMPL, CW27S1KPJZ, WS27S1KTPI, ZS27S1KWD4, ZY27AL149W, AG27ANNN5T. Licenses for supplementary figures: *UJ276VPQK0, GI276VPOCW, YV27819I1A, MT277FW9XW.*

SUPPLEMENTARY FIGURES

Supplementary Figure 1. Unprocessed G0 confocal images

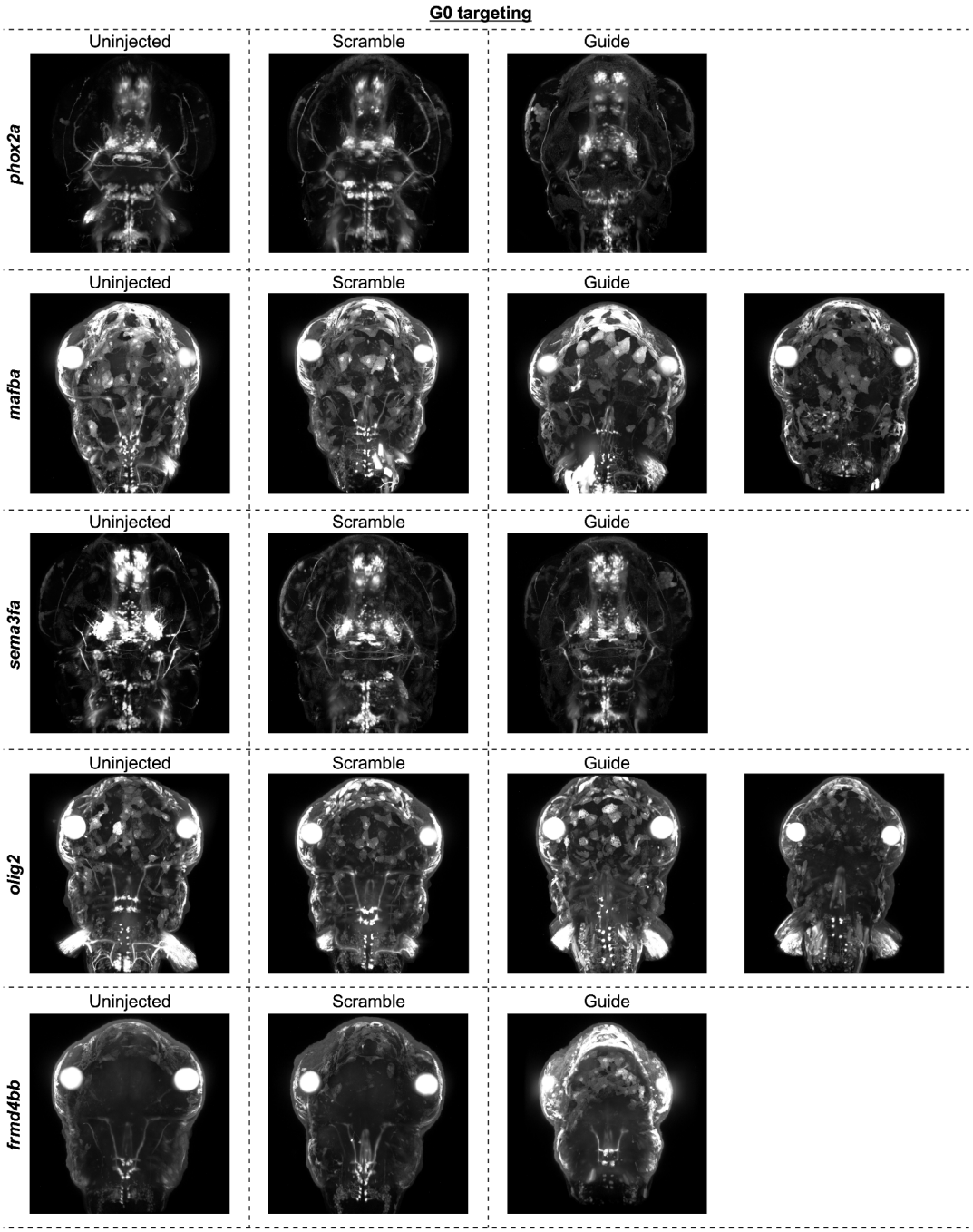

For each tested gene (named on the far left side of the figure), uninjected (left), scramble guide-injected (middle), and gene-targeting guide-injected (right) zebrafish on the appropriate reporter line backgrounds were imaged using confocal microscopy. Unprocessed confocal images are shown here and demonstrate autofluorescence of the skin and eyes, which in some cases obscure anatomical structures of interest. While non-ocular abnormalities were observed in some mutants (e.g., malformation of spinal and vagus motor neurons in *mafba* and *olig2* mutants), these were not the primary phenotypes assessed by our screen.

Supplementary Figure 2. Unprocessed F2 confocal images

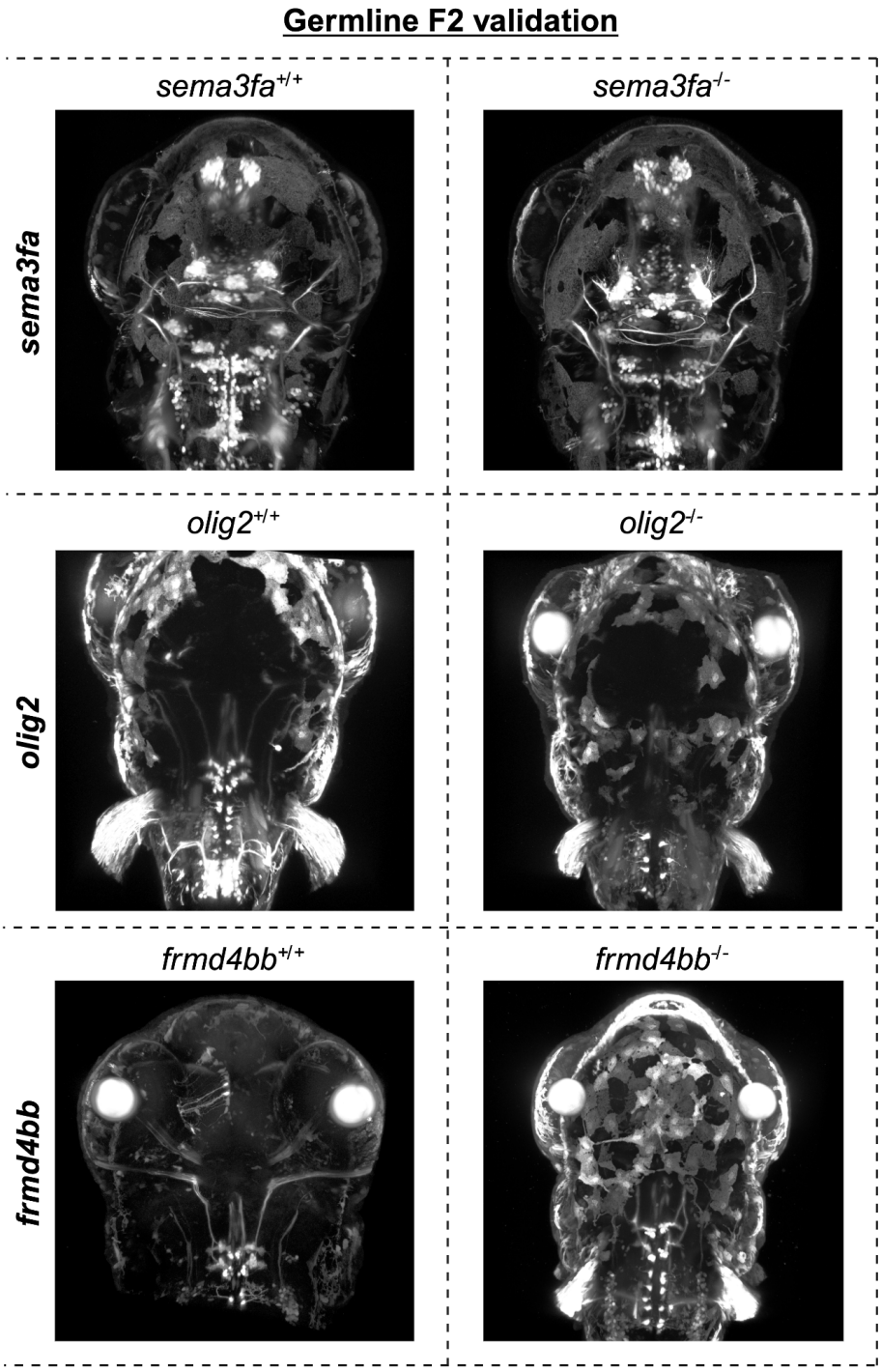

For each tested gene (named on the far left side of the figure), wild-type (left) and homozygous null (right) mutant zebrafish on the appropriate reporter line backgrounds were imaged using confocal microscopy. Unprocessed confocal images are shown here and demonstrate autofluorescence of the skin and eyes, which in some cases obscure anatomical structures of interest. While non-ocular abnormalities were observed in some mutants (e.g., malformation of spinal and vagus motor neurons in *mafba* and *olig2* mutants), these were not the primary phenotypes assessed by our screen.

Supplementary Figure 3. Stereomicroscope images of sema3fa- and frmd4bb-targeted G0 fish

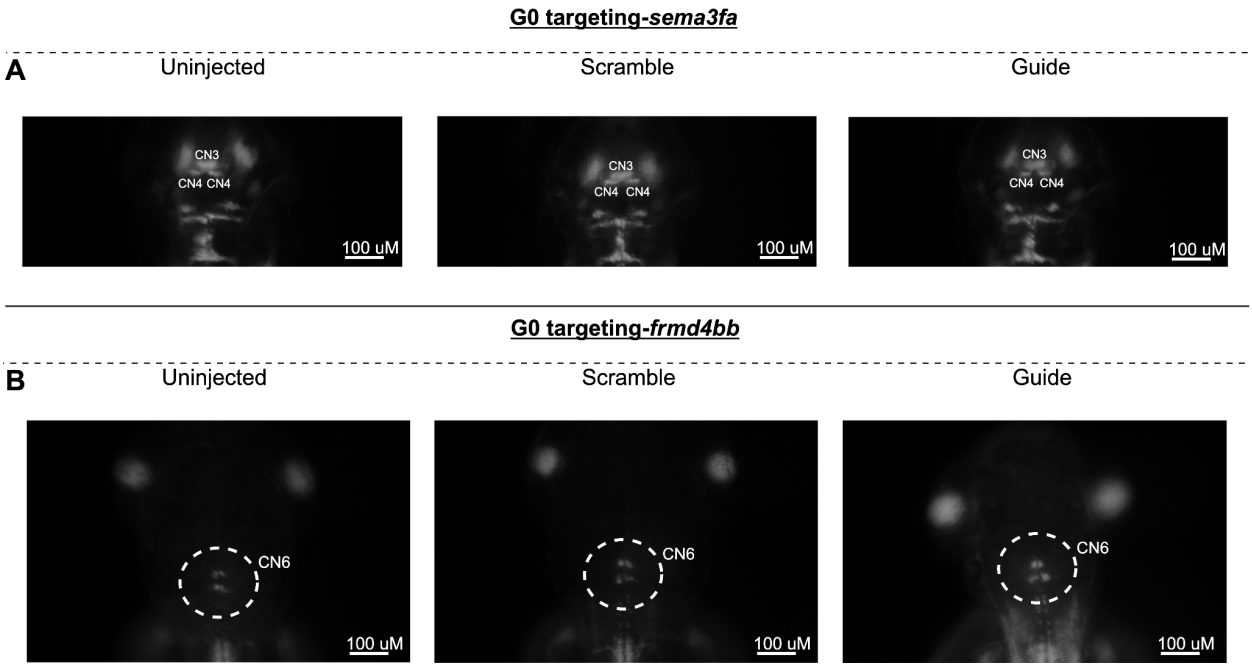

For each tested gene (named on the far left side of the figure), uninjected (left), scramble guide-injected (middle), and gene-targeting guide-injected (right) zebrafish on the appropriate reporter line backgrounds were imaged in a single z-plane on the stereomicroscope. While phenotypes including axonal defasciculation (*sema3fa*) or condensation of the columns of the motor nuclei and shortened nerves (*frmd4bb*) were visible under the stereomicroscope, these appeared more subtle than the obvious motor neuron loss phenotypes and required manual adjustment of the focus up and down in z-space to visualize. For this reason, confocal imaging was required to encapsulate the phenotypes of these mutants.

Supplementary Figure 4. 2D protein structural mapping of SEMA3F and FRMD4B

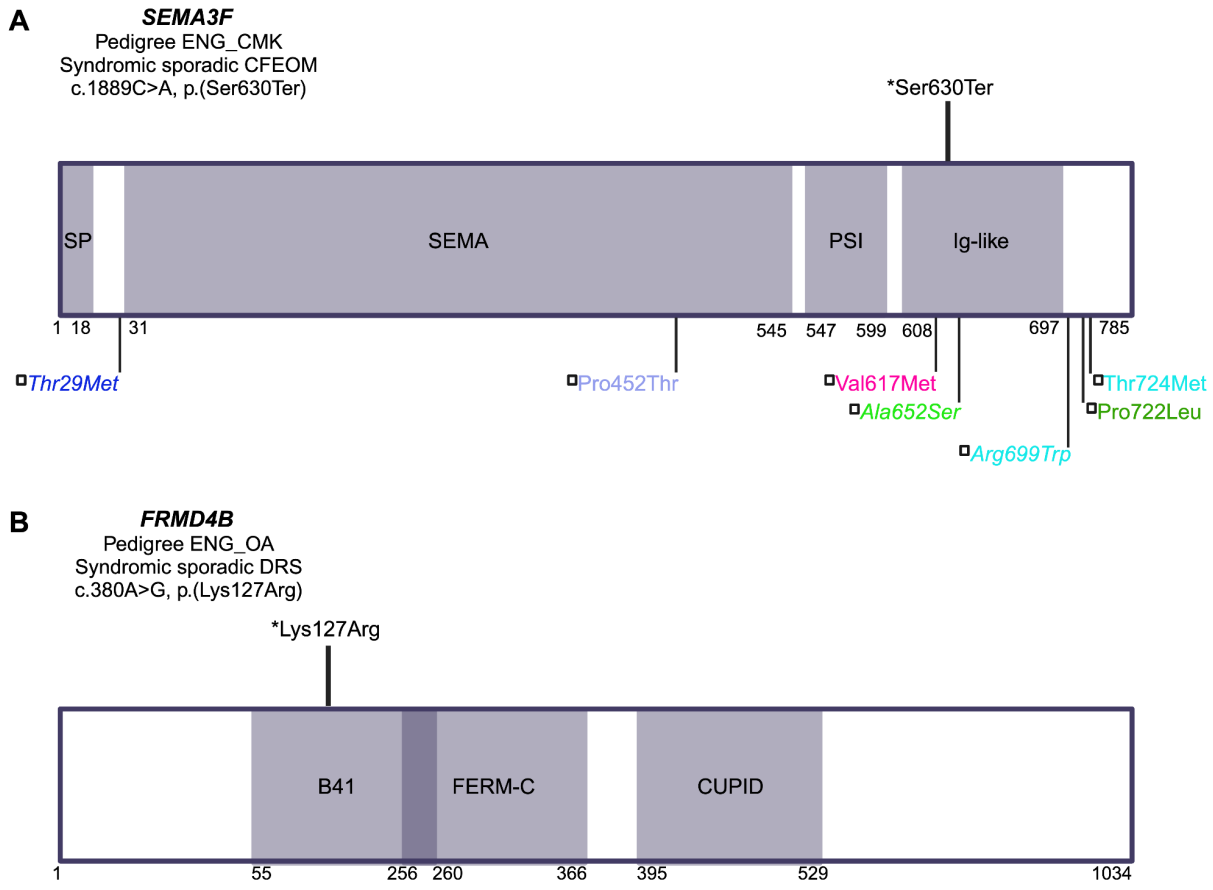

2D structural mapping of human variants. A: Variants in SEMA3F associated with CFEOM and/or other SEMA3F-associated phenotypes. B: Variants in FRMD4B associated with DRS. Key: *Variants above schematics and colored in black were initially identified and reported in our sequenced human oCCDD cohort[1] and LOF of these genes is tested for the first time in zebrafish in this work: **A)** *SEMA3F* c.1889C>A, p.(Ser630Ter) with CFEOM + sensorineural hearing loss + developmental delay + brain malformations + mild facial dysmorphisms + shortening and contractures of the fingers, and **B)** *FRMD4B* c.380A>G, p.(Lys127Arg) with DRS + hearing impairment + delayed speech and walking + atrial septal defect + gastrointestinal abnormalities. **A)** -Variants below schematic are previously reported heterozygous SEMA3F missense variants, colored as follows: dark blue denotes reproductive system phenotype + anosmia/ hyposmia + obese/ overweight; light blue denotes +/- reproductive system phenotype +/- anosmia/ hyposmia +/- obese/ overweight; lime green denotes reproductive system phenotype + anosmia/ hyposmia; cyan denotes reproductive system phenotype; dark green denotes reproductive system phenotype + obese/overweight.[16] Note that three italicized variants from this reported SEMA3F case series (SEMA3F p.(Thr29Met), p.(Ala652Ser), and p.(Arg699Trp)) also carried variants of uncertain significance in additional genes known to be associated with the probands' conditions *(CHD7* and *IGSF10; FGFR1;* and *TACR3,* respectively). The probands' specific alleles in each of these three genes had each been reported in the literature in at least one additional unrelated proband with similar phenotypes. Magenta denotes hearing impairment (ClinVar Variation ID: 1064910).[16] Variants are mapped using the following transcripts: ENST00000002829.8 (SEMA3F), ENST00000398540.8 (FRMD4B). Abbreviations: B41- band 4.1 domain, CFEOM- congenital fibrosis of the extraocular muscles, CUPID- cytohesin ubiquitin protein inducing domain, DRS- Duane retraction syndrome, FERM-C- FERM C-terminal PH-like domain, Ig-like- immunoglobulin-like domain, PSI- plexin semaphorin integrin homology domain, SEMA- semaphorin domain, SP- signal peptide region.

SUPPLEMENTARY REFERENCES

1. Jurgens JA, Barry BJ, Chan WM, et al. Expanding the genetics and phenotypes of ocular congenital cranial dysinnervation disorders. *Genet Med*. Published online July 18, 2024:101216.

2. Untergasser A, Cutcutache I, Koressaar T, et al. Primer3--new capabilities and interfaces. *Nucleic Acids Res*. 2012;40(15):e115.

3. Kent WJ. BLAT--the BLAST-like alignment tool. *Genome Res*. 2002;12(4):656-664.

4. Richards S, Aziz N, Bale S, et al. Standards and guidelines for the interpretation of sequence variants: a joint consensus recommendation of the American College of Medical Genetics and Genomics and the Association for Molecular Pathology. *Genet Med*. 2015;17(5):405-424.

5. Ioannidis NM, Rothstein JH, Pejaver V, et al. REVEL: An Ensemble Method for Predicting the Pathogenicity of Rare Missense Variants. *Am J Hum Genet*. 2016;99(4):877-885.

6. Labun K, Montague TG, Krause M, Torres Cleuren YN, Tjeldnes H, Valen E. CHOPCHOP v3: expanding the CRISPR web toolbox beyond genome editing. *Nucleic Acids Res*. 2019;47(W1):W171-W174.

7. Labun K, Montague TG, Gagnon JA, Thyme SB, Valen E. CHOPCHOP v2: a web tool for the next generation of CRISPR genome engineering. *Nucleic Acids Res*. 2016;44(W1):W272-W276.

8. Montague TG, Cruz JM, Gagnon JA, Church GM, Valen E. CHOPCHOP: a CRISPR/Cas9 and TALEN web tool for genome editing. *Nucleic Acids Res*. 2014;42(Web Server issue):W401-W407.

9. Wu RS, Lam II, Clay H, Duong DN, Deo RC, Coughlin SR. A Rapid Method for Directed Gene Knockout for Screening in G0 Zebrafish. *Dev Cell*. 2018;46(1):112-125.e4.

10. Popp MW, Maquat LE. Leveraging Rules of Nonsense-Mediated mRNA Decay for Genome Engineering and Personalized Medicine. *Cell*. 2016;165(6):1319-1322.

11. Varshney GK, Carrington B, Pei W, et al. A high-throughput functional genomics workflow based on CRISPR/Cas9-mediated targeted mutagenesis in zebrafish. *Nat Protoc*. 2016;11(12):2357-2375.

12. Rácz A, Allan B, Dwyer T, Thambithurai D, Crespel A, Killen SS. Identification of Individual Zebrafish (): A Refined Protocol for VIE Tagging Whilst Considering Animal Welfare and the Principles of the 3Rs. *Animals (Basel)*. 2021;11(3). doi:10.3390/ani11030616

13. Higashijima S, Hotta Y, Okamoto H. Visualization of cranial motor neurons in live transgenic zebrafish expressing green fluorescent protein under the control of the islet-1 promoter/enhancer. *J Neurosci*. 2000;20(1):206-218.

14. Asakawa K, Higashijima SI, Kawakami K. An mnr2b/hlxb9lb enhancer trap line that labels spinal and abducens motor neurons in zebrafish. *Dev Dyn*. 2012;241(2):327-332.

15. Paysan-Lafosse T, Blum M, Chuguransky S, et al. InterPro in 2022. *Nucleic Acids Res*.

2023;51(D1):D418-D427.

16. Landrum MJ, Lee JM, Benson M, et al. ClinVar: improving access to variant interpretations and supporting evidence. *Nucleic Acids Res*. 2018;46(D1):D1062-D1067.

17. Kock KH, Kimes PK, Gisselbrecht SS, et al. DNA binding analysis of rare variants in homeodomains reveals homeodomain specificity-determining residues. *Nat Commun*. 2024;15(1):3110.

18. Schneider CA, Rasband WS, Eliceiri KW. NIH Image to ImageJ: 25 years of image analysis. *Nat Methods*. 2012;9(7):671-675.

19. Berger MF, Philippakis AA, Qureshi AM, He FS, Estep PW 3rd, Bulyk ML. Compact, universal DNA microarrays to comprehensively determine transcription-factor binding site specificities. *Nat Biotechnol*. 2006;24(11):1429-1435.

20. Berger MF, Bulyk ML. Universal protein-binding microarrays for the comprehensive characterization of the DNA-binding specificities of transcription factors. *Nat Protoc*. 2009;4(3):393-411.

FIGURE 7 REFERENCES

1. Jurgens JA, Barry BJ, Chan WM, et al. Expanding the genetics and phenotypes of ocular congenital cranial dysinnervation disorders. *Genet Med*. Published online July 17, 2024:101216.

2. Nakano M, Yamada K, Fain J, et al. Homozygous mutations in ARIX(PHOX2A) result in congenital fibrosis of the extraocular muscles type 2. *Nat Genet*. 2001;29(3):315-320.

3. Khan AO, Almutlaq M, Oystreck DT, Engle EC, Abu-Amero K, Bosley T. Retinal Dysfunction in Patients with Congenital Fibrosis of the Extraocular Muscles Type 2. *Ophthalmic Genet*. 2016;37(2):130-136.

4. Dong JM, Shen Q, Li J, et al. Identification of a novel PHOX2A gene mutation in a Chinese family with congenital fibrosis of extraocular muscles type 2. *Zhonghua Yi Xue Yi Chuan Xue Za Zhi*. 2012;29(1):5-8.

5. Yazdani A, Chung DC, Abbaszadegan MR, et al. A novel PHOX2A/ARIX mutation in an Iranian family with congenital fibrosis of extraocular muscles type 2 (CFEOM2). *Am J Ophthalmol*. 2003;136(5):861-865.

6. Park JG, Tischfield MA, Nugent AA, et al. Loss of MAFB Function in Humans and Mice Causes Duane Syndrome, Aberrant Extraocular Muscle Innervation, and Inner-Ear Defects. *Am J Hum Genet*. 2016;98(6):1220-1227.

7. Pascolini G, Passarelli C, Lipari M, et al. Duane retraction syndrome characterized by inner ear agenesis and neurodevelopmental phenotype in an Italian family with a variant in MAFB. *Clin Genet*. 2022;101(3):377-378.

8. Sato Y, Tsukaguchi H, Morita H, et al. A mutation in transcription factor MAFB causes Focal Segmental Glomerulosclerosis with Duane Retraction Syndrome. *Kidney Int*. 2018;94(2):396-

407.

9. Kaimori JY, Mori T, Namba-Hamano T, et al. Cyclosporine A Treatment of Proteinuria in a New Case of MAFB-Associated Glomerulopathy without Extrarenal Involvement: A Case Report. *Nephron*. 2021;145(4):445-450.

10. Bensaid S, Bendahmane M, Loddo S, et al. Clinical and molecular cytogenetic studies of five new patients with 20q11q12 deletion and review of the literature: Proposition of two critical regions. *Am J Med Genet A*. 2024;194(7):e63580.

20. Wu RS, Lam II, Clay H, Duong DN, Deo RC, Coughlin SR. A rapid method for directed gene knockout for screening in G0 zebrafish. *Dev Cell*. 2018;46(1):112–125.e4.
21. Jao LE, Wente SR, Chen W. Efficient multiplex biallelic zebrafish genome editing using a CRISPR nuclease system. *Proc Natl Acad Sci USA*. 2013;110:13904–13909.
22. Richards S, Aziz N, Bale S, et al. Standards and guidelines for the interpretation of sequence variants: a joint consensus recommendation of the American College of Medical Genetics and Genomics and the Association for Molecular Pathology. *Genet Med*. 2015;17:405–424.
23. Rehm HL, Berg JS, Brooks LD, et al. ClinGen–the Clinical Genome Resource. *N Engl J Med*. 2015;372:2235–2242.
24. Guo S, Brush J, Teraoka H, et al. Development of noradrenergic neurons in the zebrafish hindbrain requires BMP, FGF8, and the homeodomain protein soulless/Phox2a. *Neuron*. 1999;24:555–566.
25. Barrera LA, Vedenko A, Kurland JV, et al. Survey of variation in human transcription factors reveals prevalent DNA binding changes. *Science*. 2016;351(6280):1450–1454.
26. Berger MF, Philippakis AA, Qureshi AM, He FS, Estep PW, 3rd, Bulyk ML. Compact, universal DNA microarrays to comprehensively determine transcription-factor binding site specificities. *Nat Biotechnol*. 2006;24:1429–1435.
27. Paysan-Lafosse T, Blum M, Chuguransky S, et al. InterPro in 2022. *Nucleic Acids Res*. 2023;51(D1):D418–D427.
28. Whitman MC, Engle EC. Ocular congenital cranial dysinnervation disorders (CCDDs): insights into axon growth and guidance. *Hum Mol Genet*. 2017;26(R1):R37–R44.
29. Barry BJ, Whitman MC, Hunter DG, Engle EC. Duane syndrome. In: Adam MP, Feldman J, Mirzaa GM, et al., eds. *GeneReviews*. Seattle: University of Washington; 2007.
30. Whitman MC, Miyake N, Nguyen EH, et al. Decreased ACKR3 (CXCR7) function causes oculomotor synkinesis in mice and humans. *Hum Mol Genet*. 2019;28:3113–3125.
31. Yazdani A, Chung DC, Abbaszadegan MR, et al. A novel PHOX2A/ARIX mutation in an Iranian family with congenital fibrosis of extraocular muscles type 2 (CFEOM2). *Am J Ophthalmol*. 2003;136:861–865.
32. Sato Y, Tsukaguchi H, Morita H, et al. A mutation in transcription factor MAFB causes focal segmental glomerulosclerosis with duane retraction syndrome. *Kidney Int*. 2018;94:396–407.
33. Kaimori JY, Mori T, Namba-Hamano T, et al. Cyclosporine a treatment of proteinuria in a new case of MAFB-associated glomerulopathy without extrarenal involvement: a case report. *Nephron*. 2021;145:445–450.
34. Bensaid S, Bendahmane M, Loddo S, et al. Clinical and molecular cytogenetic studies of five new patients with 20q11q12 deletion and review of the literature: proposition of two critical regions. *Am J Med Genet A*. 2024;194(7):e63580.
35. Pascolini G, Passarelli C, Lipari M, et al. Duane retraction syndrome characterized by inner ear agenesis and neurodevelopmental phenotype in an Italian family with a variant in MAFB. *Clin Genet*. 2022;101:377–378.
36. Sahay A, Molliver ME, Ginty DD, Kolodkin AL. Semaphorin 3F is critical for development of limbic system circuitry and is required in neurons for selective CNS axon guidance events. *J Neurosci*. 2003;23:6671–6680.
37. Bowl MR, Simon MM, Ingham NJ, et al. A large scale hearing loss screen reveals an extensive unexplored genetic landscape for auditory dysfunction. *Nat Commun*. 2017;8(1):886.
38. Landrum MJ, Lee JM, Benson M, et al. ClinVar: improving access to variant interpretations and supporting evidence. *Nucleic Acids Res*. 2018;46(D1):D1062–D1067.
39. Kotan LD, Ternier G, Cakir AD, et al. Loss-of-function variants in SEMA3F and PLXNA3 encoding semaphorin-3F and its receptor plexin-A3 respectively cause idiopathic hypogonadotropic hypogonadism. *Genet Med*. 2021;23:1008–1016.
40. Zannino DA, Appel B. Olig2+ precursors produce abducens motor neurons and oligodendrocytes in the zebrafish hindbrain. *J Neurosci*. 2009;29:2322–2333.
41. Shringarpure SS, Wang W, Jiang Y, et al. Large-scale transethnic replication and discovery of genetic associations for rare diseases with self-reported medical data. *medRxiv*. 2021-06.
42. Kong Y, Zhao L, Charette JR, et al. An FRMD4B variant suppresses dysplastic photoreceptor lesions in models of enhanced S-cone syndrome and of Nrl deficiency. *Hum Mol Genet*. 2018;27:3340–3352.
43. Cordes SP, Barsh GS. The mouse segmentation gene kr encodes a novel basic domain-leucine zipper transcription factor. *Cell*. 1994;79:1025–1034.
44. Manzanares M, Cordes S, Kwan CT, Sham MH, Barsh GS, Krumlauf R. Segmental regulation of Hoxb-3 by kreisler. *Nature*. 1997;387(6629):191–195.
45. Manzanares M, Cordes S, Ariza-McNaughton L, et al. Conserved and distinct roles of Kreisler in regulation of the paralogous Hoxa3 and Hoxb3 genes. *Development*. 1999;126:759–769.
46. Manzanares M, Trainor PA, Nonchev S, et al. The role of Kreisler in segmentation during hindbrain development. *Dev Biol*. 1999;211(2):220–237.
47. Moens CB, Yan YL, Appel B, Force AG, Kimmel CB. Valentino: a zebrafish gene required for normal hindbrain segmentation. *Development*. 1996;122:3981–3990.
48. Novitch BG, Chen AI, Jessell TM. Coordinate regulation of motor neuron subtype identity and pan-neuronal properties by the bHLH repressor Olig2. *Neuron*. 2001;31:773–789.
49. Hasan KB, Agarwala S, Ragsdale CW. PHOX2A regulation of oculomotor complex nucleogenesis. *Development*. 2010;137:1205–1213.
50. Mazzoni EO, Mahony S, Closser M, et al. Synergistic binding of transcription factors to cell-specific enhancers programs motor neuron identity. *Nat Neurosci*. 2013;16:1219–1227.

Investigative Ophthalmology & Visual Science